Chap.2 Stellar populations and chemical evolution

- Stars in a color-magnitude diagram
  - nearby stars, globular clusters
- Stellar evolution and population synthesis
  - evolutionary tracks, metallicity vs. age
  - star formation, single starburst model
- Origin of elements and yields
  - Supernovae and hypernovae
- Extremely metal-poor stars
  - Neutron capture elements, CEMP stars
- Galactic chemical evolution
  - IMF, SFR, Simple model, G-dwarf problem

1. Stars in a color-magnitude diagram (CMD)

CMD for nearby stars with Hipparcos satellite (1989~1993)

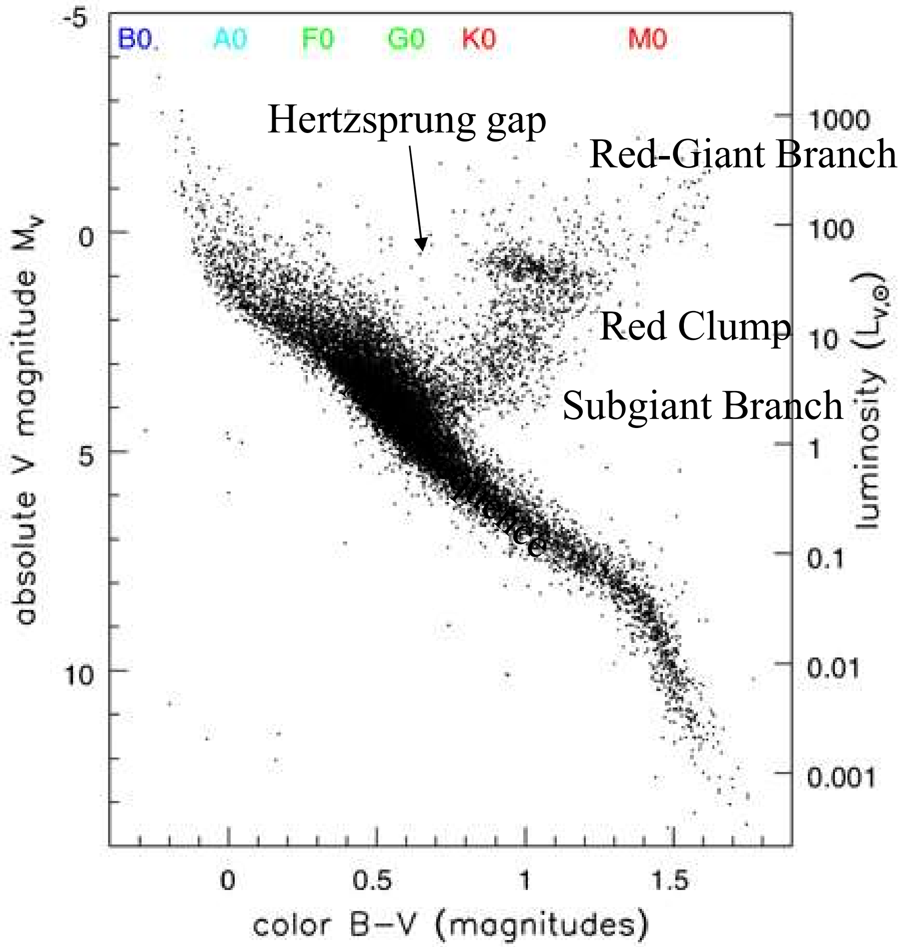

Fig 2.2 (Hipparcos)'Galaxies in the Universe' Sparke/Gallagher CUP 2007

Mv from trigonometric distances = $1/\pi$ (where relative error in parallax $\Delta\pi$ <10%)

Many young stars
+ some old stars

Astrometry Satellites

	1989~1993	2013~
	Hipparcos	**Gaia**
Magnitude limit	12 mag	20 mag
Completeness	7.3 – 9.0 mag	20 mag
Bright limit	0 mag	6 mag
Number of objects	120,000	26 million to V = 15 250 million to V = 18 1000 million to V = 20
Effective distance	1 kpc	50 kpc
Quasars	1 (3C 273)	500,000
Galaxies	None	1,000,000
Accuracy	1 milliarcsec	7 μarcsec at V = 10 10 – 25 μarcsec at V = 15 300 μarcsec at V = 20
Photometry	2-colour (B and V)	Low-res. spectra to V = 20
Radial velocity	None	15 km s^{-1} to V = 17
Observing	Pre-selected	Complete and unbiased

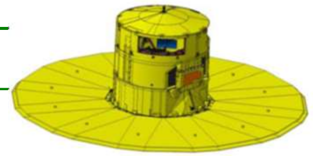

~10μas

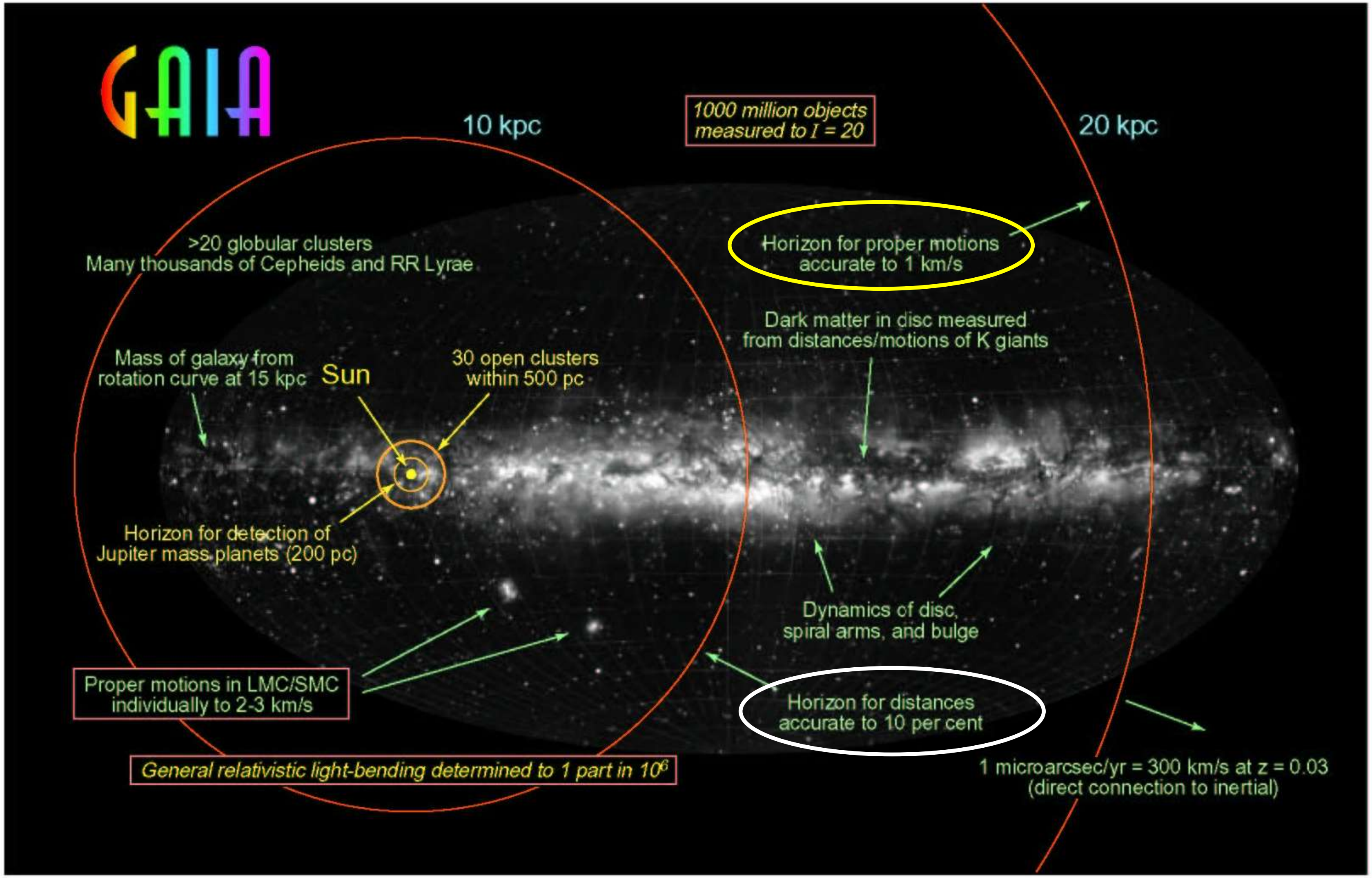

Gaia: 10μas = 10% error @distance 10kpc, 10μas/yr = 1km/s @20kpc

Hipparcos: 1mas = 10% error @distance 100pc, 1mas/yr = 5km/s @ 1kpc

The Map of the Milky Way with Gaia

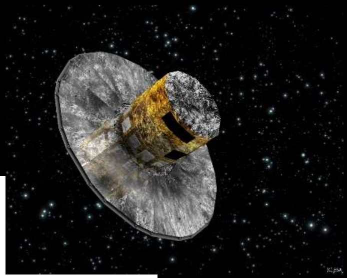

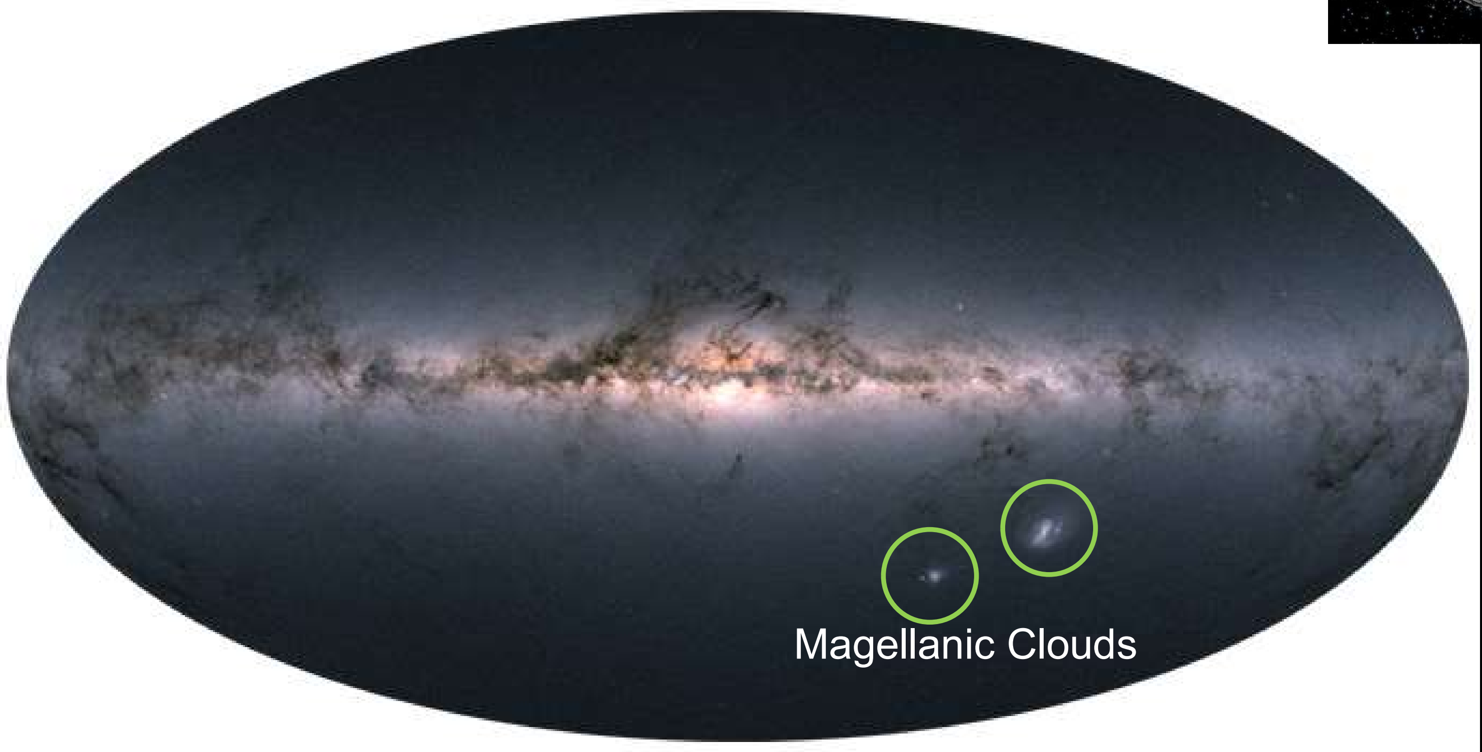

CMD for nearby stars with Gaia

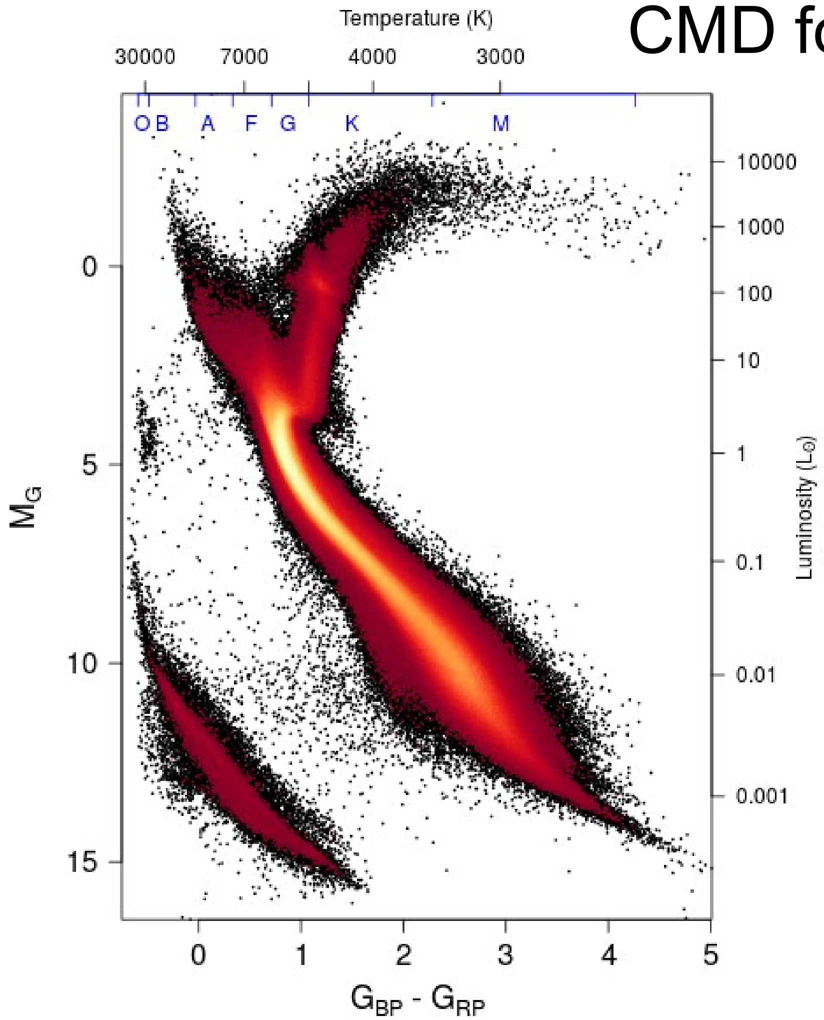

Gaia HRD of sources with low extinction (E(B − V) < 0.015 mag) satisfying the filters described in Sect. 2.1 (4,276,690 stars). The colour scale represents the square root of the density of stars. Approximate temperature and luminosity equivalents for main-sequence stars are provided at the top and right axis, respectively, to guide the eye.

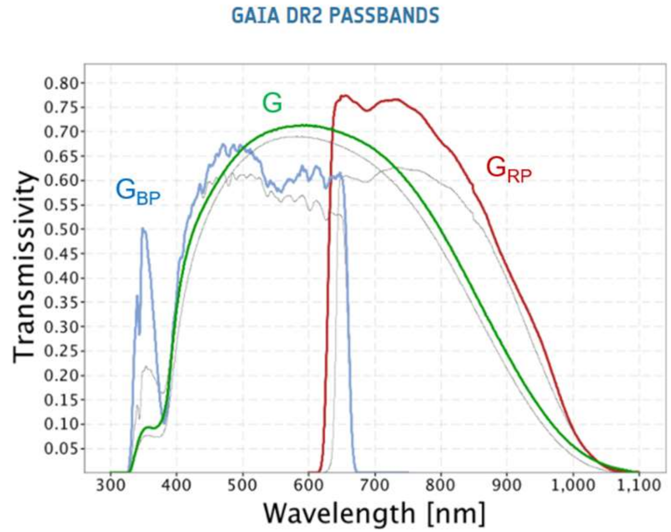

The coloured lines in the figure show the revised passbands for G, G_{BP} and G_{RP} (green: G; blue: G_{BP}; red: G_{RP}), defining the Gaia DR2 photometric system. The thin, grey lines show the nominal, pre-launch passbands published in Jordi et al. 2010, used for Gaia DR1.

Photometric Systems

M. Bessel 2005 ARAA, 43, 293

TABLE 1 Wavelengths (Å) and widths (Å) of broad-band systems

UBVRI			Washington			SDSS			Hipparcos			WFPC2		
	λeff	Δλ		λeff	Δλ		λeff	Δλ		λeff	Δλ		λeff	Δλ
U	3663	650	C	3982	1070	u'	3596	570	H_P	5170	2300	F336	3448	340
B	4361	890	M	5075	970	g'	4639	1280	B_T	4217	670	F439	4300	720
V	5448	840	T_1	6389	770	r'	6122	1150	V_T	5272	1000	F555	5323	1550
R	6407	1580	T_2	8051	1420	i'	7439	1230				F675	6667	1230
I	7980	1540				z'	8896	1070				F814	7872	1460

TABLE 3 Wavelengths (Å) and widths (Å) of intermediate-band systems

Strömgren			DDO			Geneva			Vilnius			Walraven		
	λeff	Δλ		λeff	Δλ		λeff	Δλ		λeff	Δλ		λeff	Δλ
u	3520	314	35	3460	383	U	3438	170	U	3450	400	W	3255	143
v	4100	170	38	3815	330	B	4248	283	P	3740	260	U	3633	239
b	4688	185	41	4166	83	$B1$	4022	171	X	4050	220	L	3838	227
y	5480	226	42	4257	73	$B2$	4480	164	Y	4660	260	B	4325	449
β_w	4890	150	45	4517	76	V	5508	298	Z	5160	210	V	5467	719
β_n	4860	30	48	4886	186	$V1$	5408	202	V	5440	260			
			51	5132	162	G	5814	206	S	6560	200			

Photometric Systems

M. Bessel 2005 ARAA, 43, 293

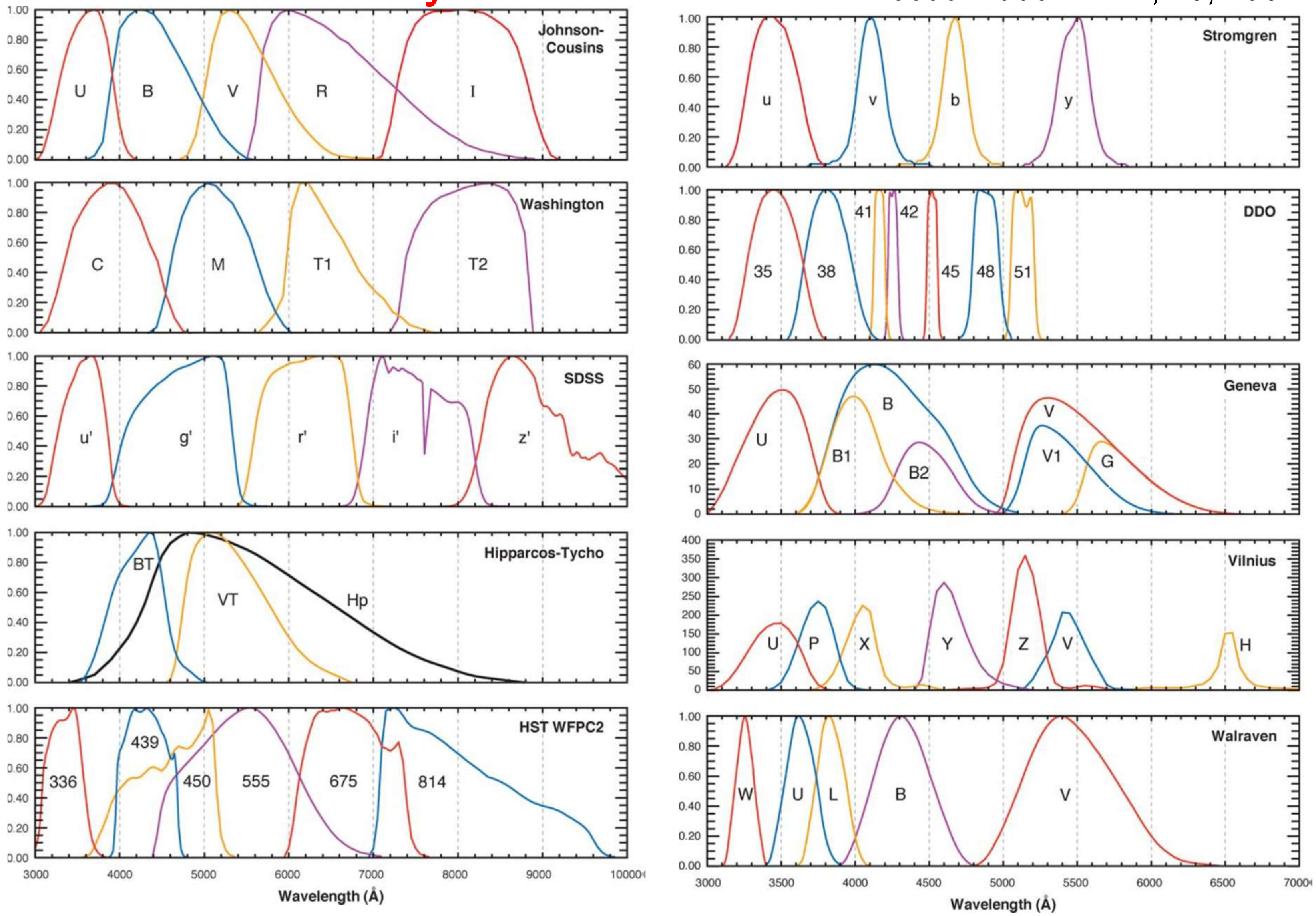

HSC broad-band filters

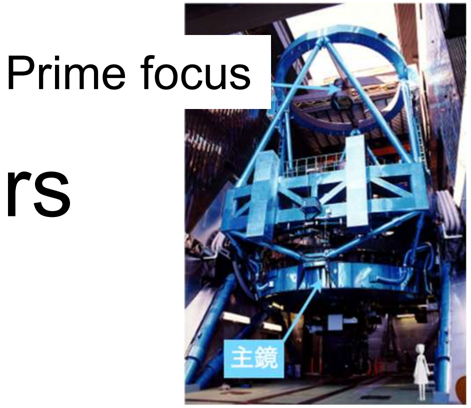

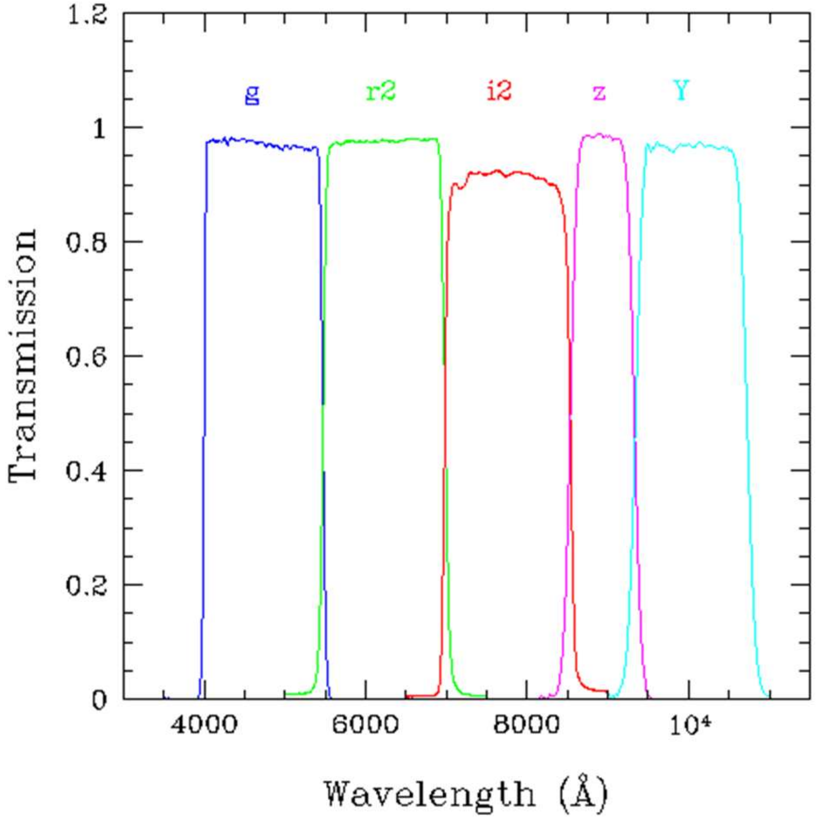

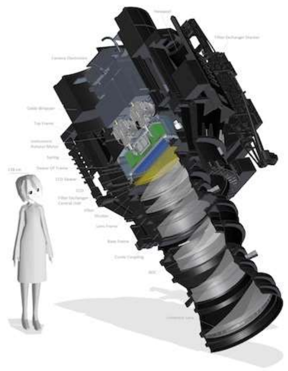

CMD for a Galactic globular cluster

M68
[Fe/H]= -1.99

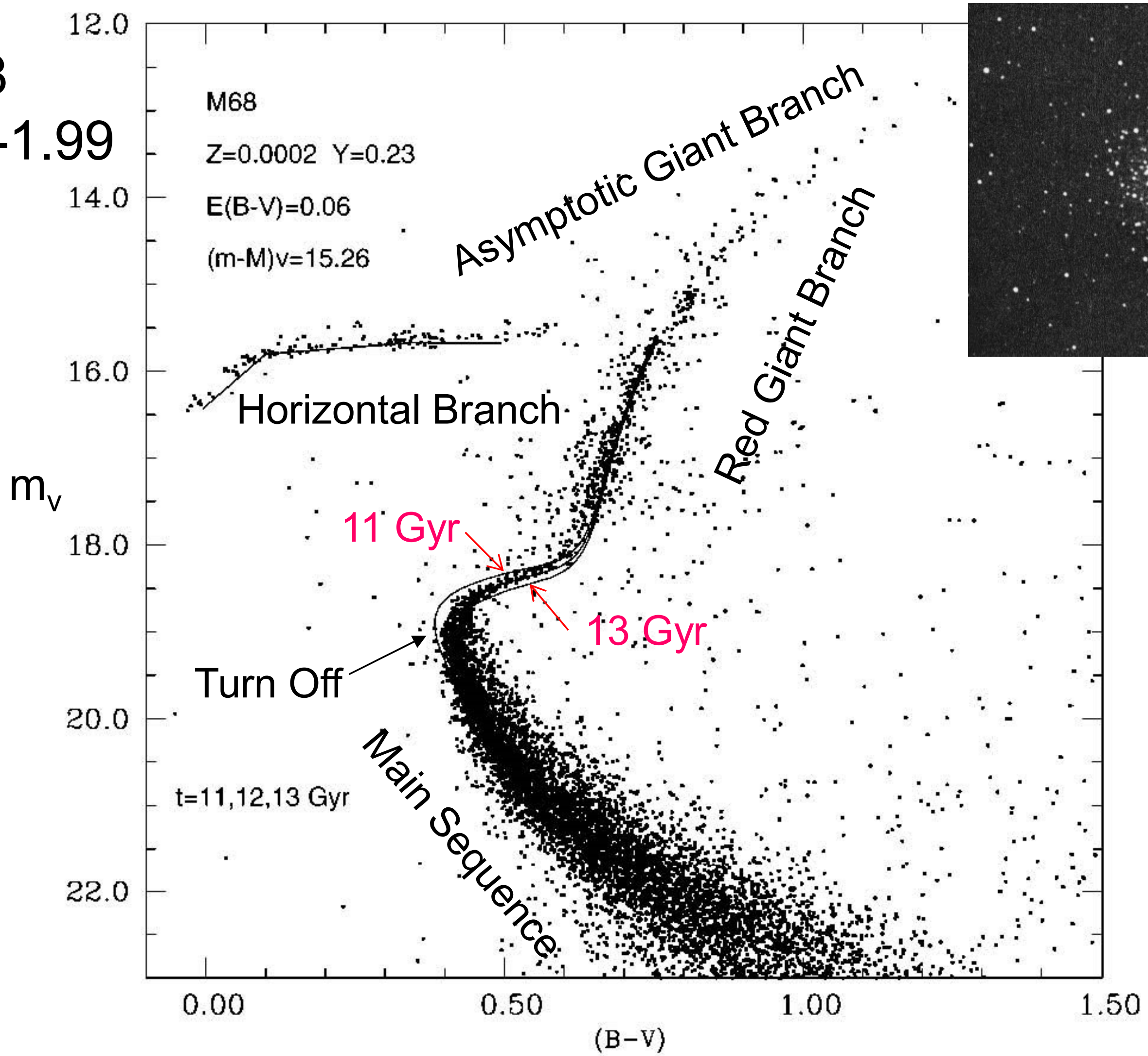

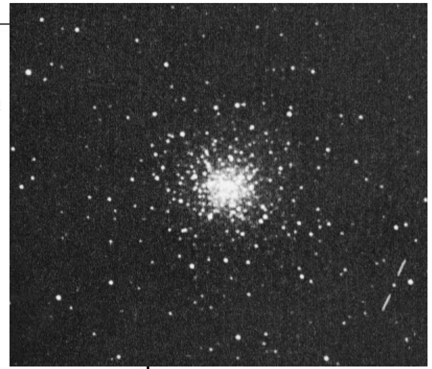

CM diagrams for Galactic globular clusters

M3
[Fe/H]= -1.57

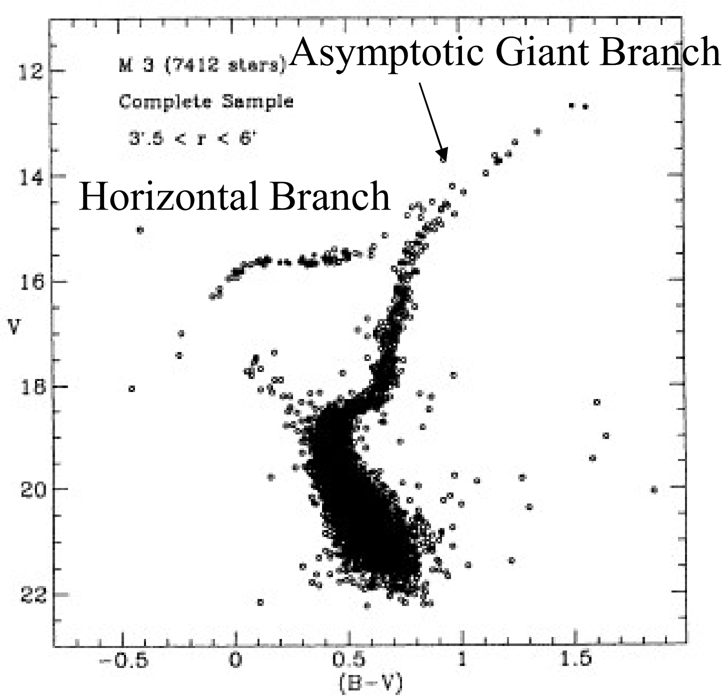

47 Tuc
[Fe/H]= -0.76

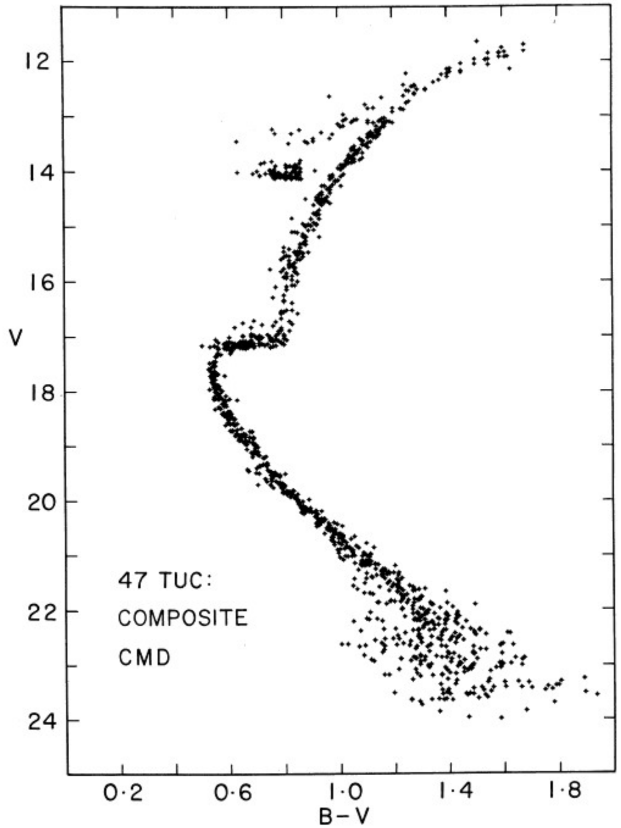

2. Stellar evolution and population synthesis

Evolutionary tracks

Iben 1967, ARAA, 5, 571

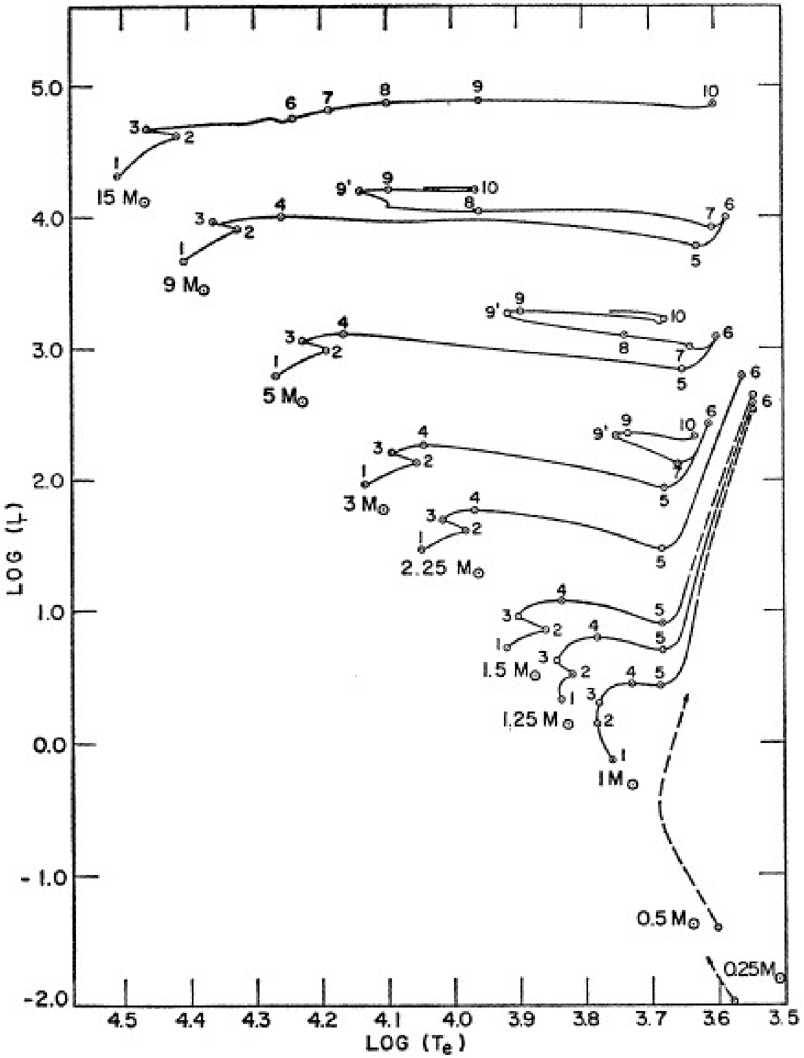

TABLE III

Stellar Lifetimes (yr)[a]

Mass ($M_\odot$) \ Interval ($i-j$)	(1–2)	(2–3)	(3–4)	(4–5)	(5–6)
15	1.010 (7)	2.270 (5)		7.55 (4)	
9	2.144 (7)	6.053 (5)	9.113 (4)	1.477 (5)	6.552 (4)
5	6.547 (7)	2.173 (6)	1.372 (6)	7.532 (5)	4.857 (5)
3	2.212 (8)	1.042 (7)	1.033 (7)	4.505 (6)	4.238 (6)
2.25	4.802 (8)	1.647 (7)	3.696 (7)	1.310 (7)	3.829 (7)
1.5	1.553 (9)	8.10 (7)	3.490 (8)	1.049 (8)	≥2 (8)
1.25	2.803 (9)	1.824 (8)	1.045 (9)	1.463 (8)	≥4 (8)
1.0	7 (9)	2 (9)	1.20 (9)	1.57 (8)	≥1 (9)

[a] Numbers in parentheses beside each entry give the power of ten to which that entry is to be raised.

TABLE IV

Stellar Lifetimes (yr)[a]

Mass ($M_\odot$) \ Interval ($i-j$)	(6–7)	(7–8)	(8–9)	(9–10)
15	7.17 (5)	6.20 (5)	1.9 (5)	3.5 (4)
9	4.90 (5)	9.50 (4)	3.28 (6)	1.55 (5)
5	6.05 (6)	1.02 (6)	9.00 (6)	9.30 (5)
3	2.51 (7)	4.08 (7)		6.00 (6)

[a] Numbers in parentheses beside each entry give the power of ten to which that entry is to be raised.

M ≥ 0.08 Msun : nuclear reaction
≥ 1.1 Msun : convective core, CNO
≤ 2 Msun : helium flash (T_c~10^8K)
≥ 8 Msun : C core burning

$$\left\{ \begin{array}{l} \dfrac{dP}{dr} = -\rho \dfrac{GM(<r)}{r^2} \\ M(<r) = \displaystyle\int_0^r 4\pi r^2 \rho(r) dr \Rightarrow \dfrac{dM(<r)}{dr} = 4\pi r^2 \rho \\ \Rightarrow \dfrac{dP}{dM(<r)} = -\dfrac{GM(<r)}{4\pi r^4} \end{array} \right.$$

Equation for hydrostatic equilibrium

P_c, T_c at the center

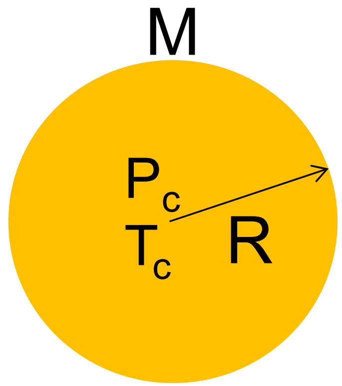

$$\frac{dP}{dM(<r)} \approx \frac{P_c}{M} \approx \frac{GM}{4\pi R^4}, P = \frac{\rho}{\mu m_H} kT,$$

Equation of state

$$T \to T_c, \rho = \frac{M}{4\pi R^3/3}, \rho_c \propto \rho$$

$$\Rightarrow T_c \propto \frac{\mu M}{R}$$

T_c is higher for larger M / smaller R

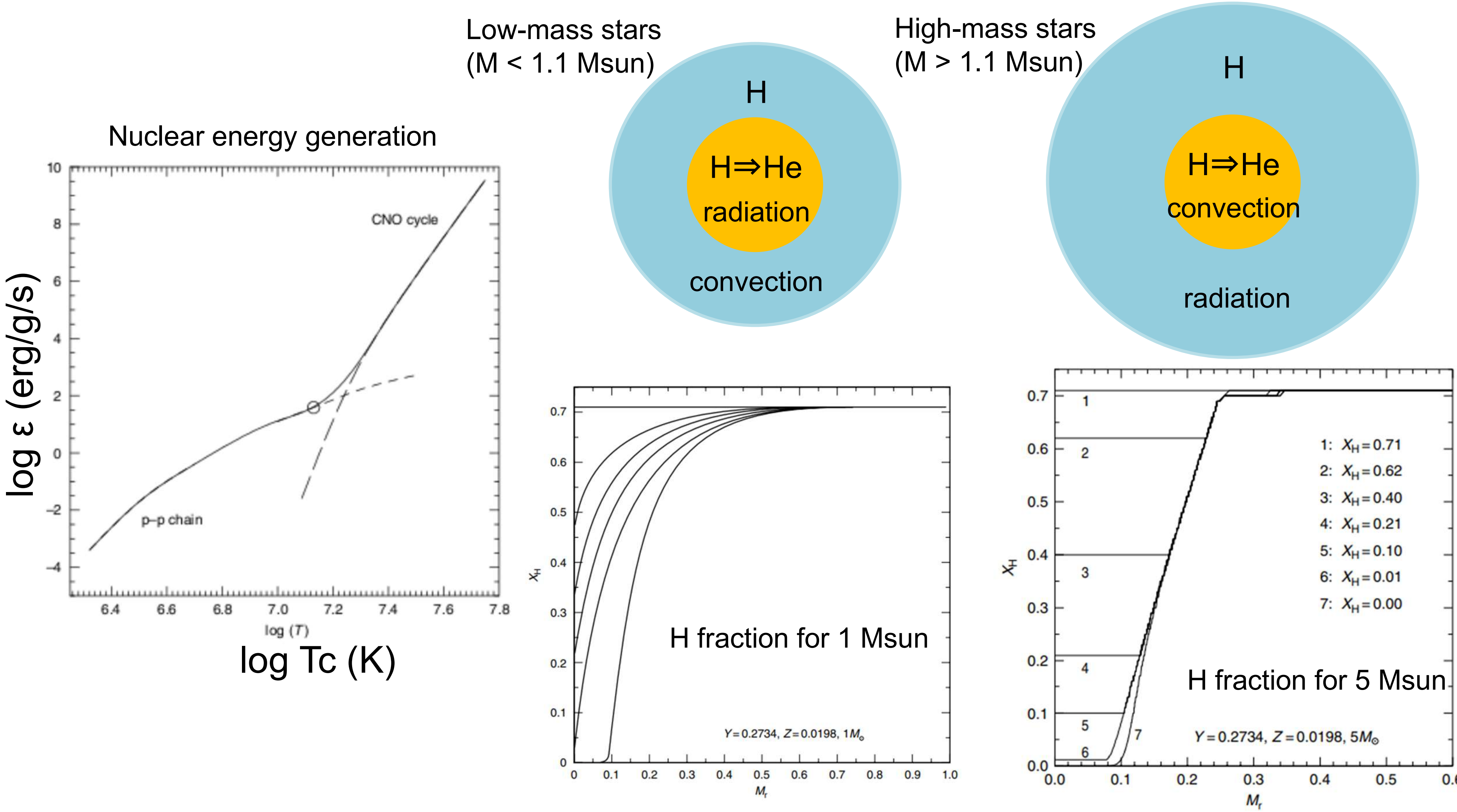
Nuclear energy generation
log ε (erg/g/s)
log Tc (K)
log (T)
CNO cycle
p–p chain
Low-mass stars
(M < 1.1 Msun)
H
H⇒He
radiation
convection
High-mass stars
(M > 1.1 Msun)
H
H⇒He
convection
radiation
H fraction for 1 Msun
Y = 0.2734, Z = 0.0198, 1M☉
H fraction for 5 Msun
Y = 0.2734, Z = 0.0198, 5M☉
1: X_H = 0.71
2: X_H = 0.62
3: X_H = 0.40
4: X_H = 0.21
5: X_H = 0.10
6: X_H = 0.01
7: X_H = 0.00

Evolutionary tracks for low/high mass stars

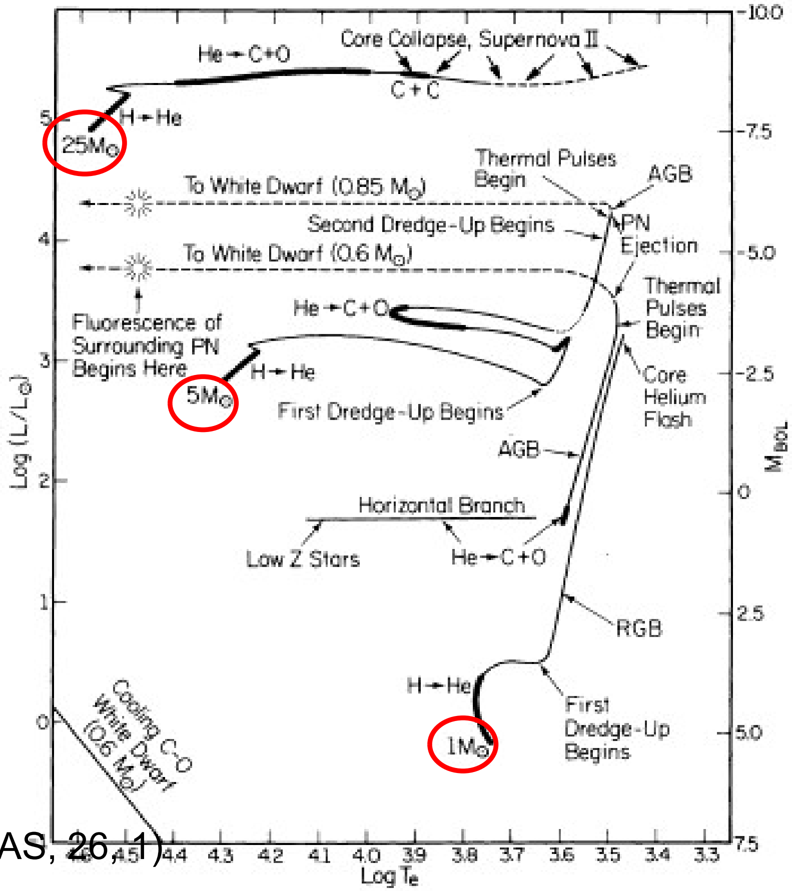

(Iben 1985, QJRAS, 26, 1)

FIG. 5.—Tracks in the H-R diagram of theoretical model stars of low (1 $M_\odot$), intermediate (5 $M_\odot$), and high (25 $M_\odot$) mass. Nuclear burning on a long time scale occurs along the heavy portions of each track. The places where first and second dredge-up episodes occur are indicated, as are the places along the AGB where thermal pulses begin. The third dredge-up process occurs during the thermal pulse phase, and it is here where one may expect the formation of carbon stars and ZrO-rich stars. The luminosity where a given track turns off from the AGB is a conjecture based on comparison with the observations. From Iben (1985).

- **Low mass, long-lived stars:** dominate stellar photometry
- **High mass, short-lived stars:** dominate stellar spectroscopy

Evolutionary track for low mass stars

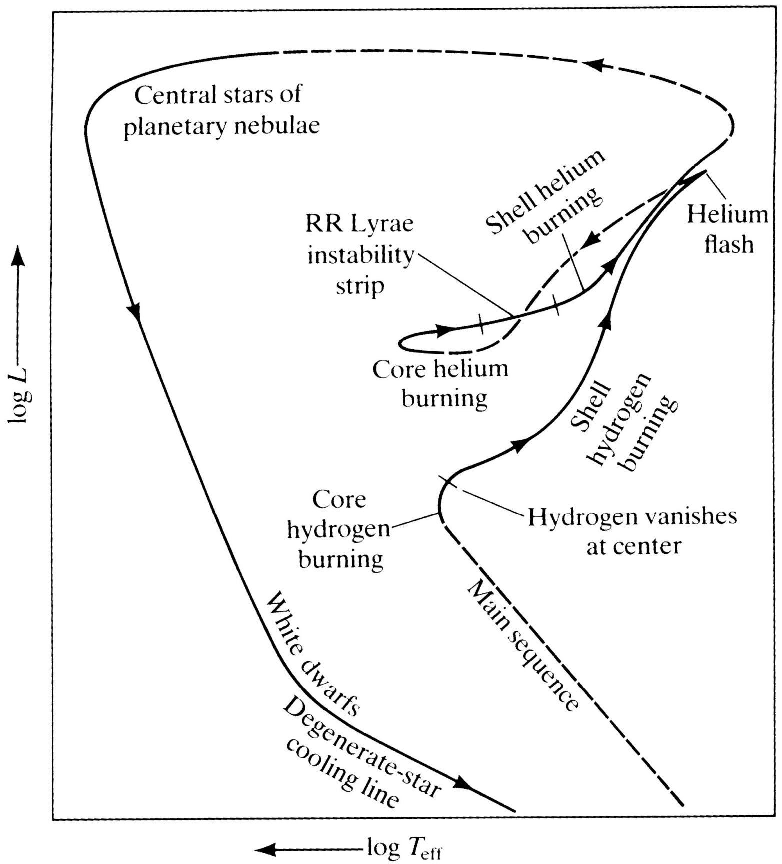

Evolutionary tracks for low/high mass stars

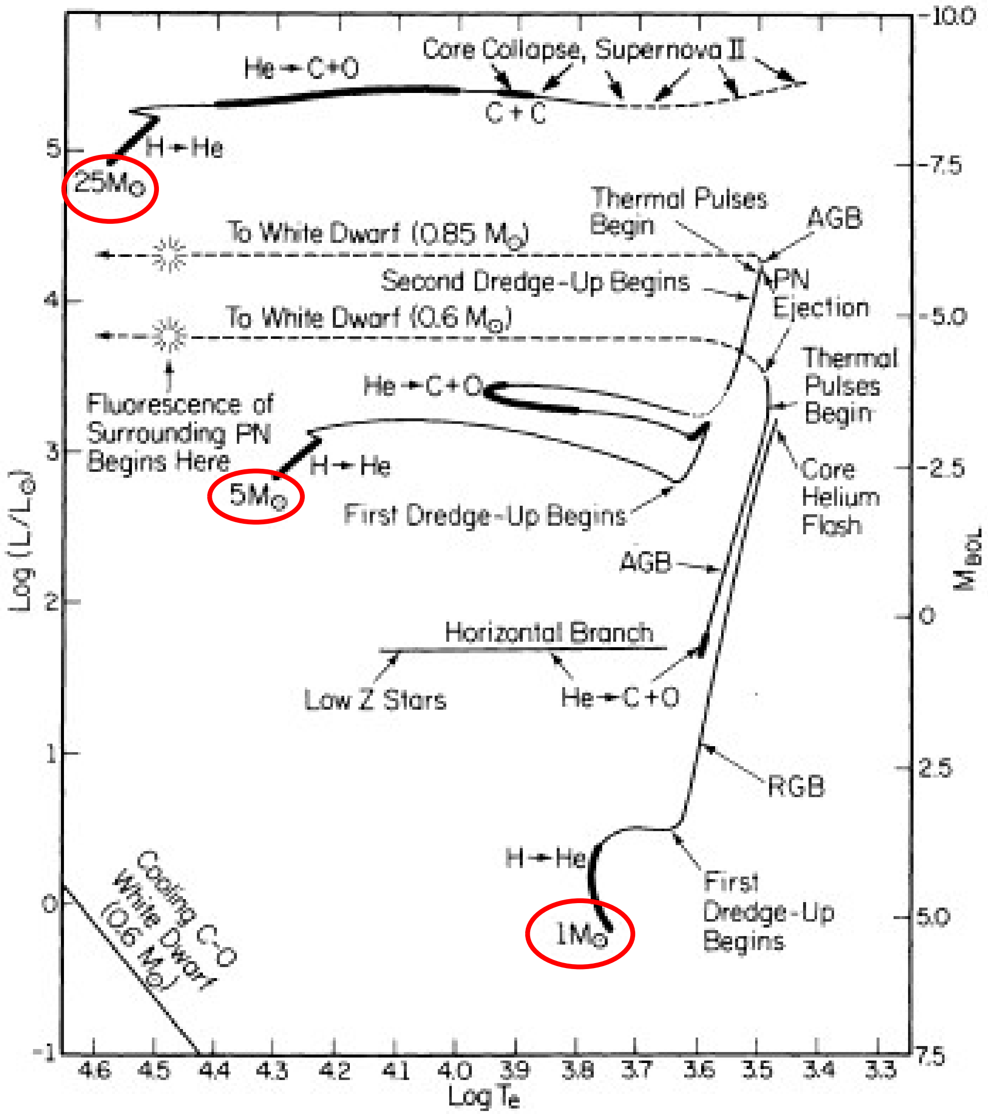

- Low mass, long-lived stars: dominate stellar photometry of old stellar systems
- High mass, short-lived stars: dominate stellar spectroscopy of old stellar systems

(Iben 1985, QJRAS, 26, 1)

FIG. 5.—Tracks in the H-R diagram of theoretical model stars of low (1 $M_\odot$), intermediate (5 $M_\odot$), and high (25 $M_\odot$) mass. Nuclear burning on a long time scale occurs along the heavy portions of each track. The places where first and second dredge-up episodes occur are indicated, as are the places along the AGB where thermal pulses begin. The third dredge-up process occurs during the thermal pulse phase, and it is here where one may expect the formation of carbon stars and ZrO-rich stars. The luminosity where a given track turns off from the AGB is a conjecture based on comparison with the observations. From Iben (1985).

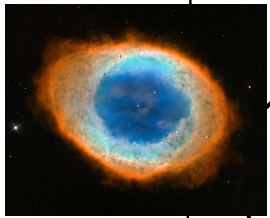

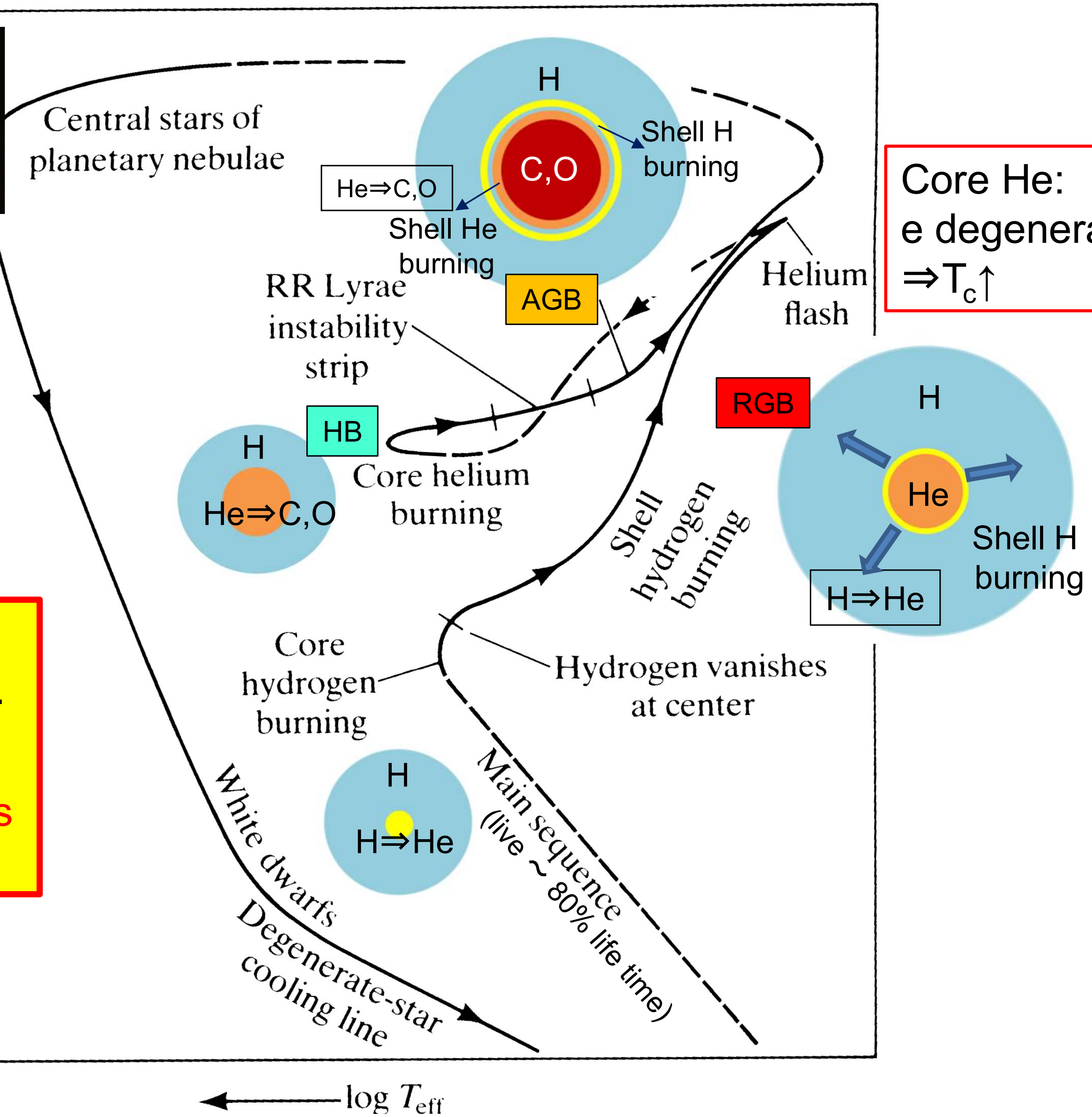

Core He:
e degeneracy
⇒T_c↑

Evolutionary track for low-mass, long-lived stars

⇒photometric properties of old stellar systems

Isochrones

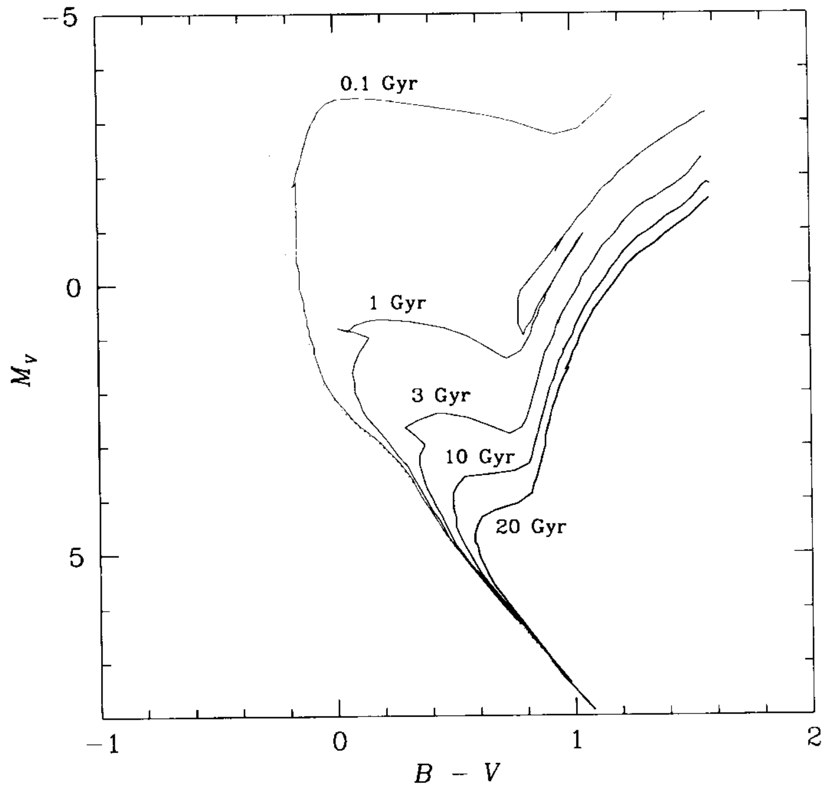

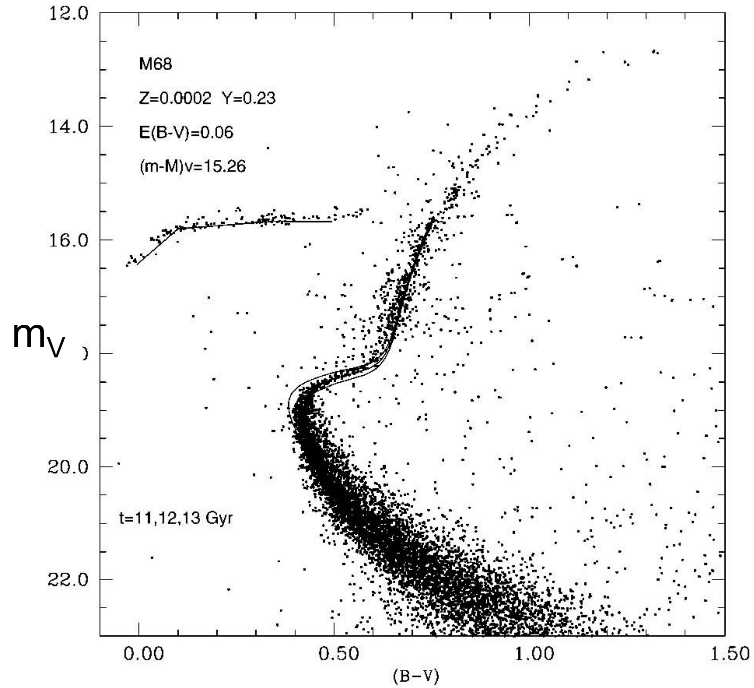

FIG. 2.—Isochrones for ages between 11 and 13 Gyr and ZAHB compared to the CMD of M68 (data from Walker 1994). Composition, distance modulus, and reddening used for the fit are given in the upper left-hand corner.

Salaris et al 1997, ApJ, 479, 665

M3
[Fe/H]= -1.57

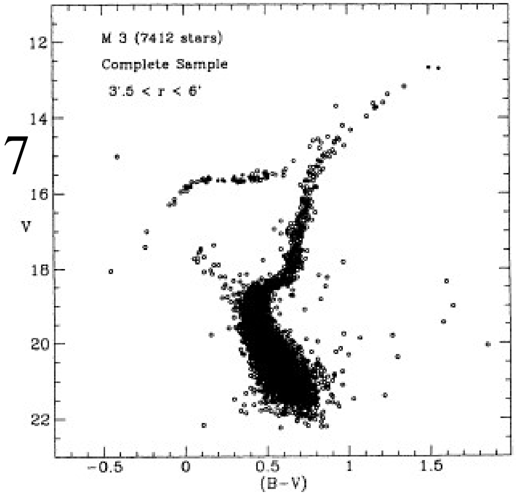

47 Tuc
[Fe/H]= -0.76

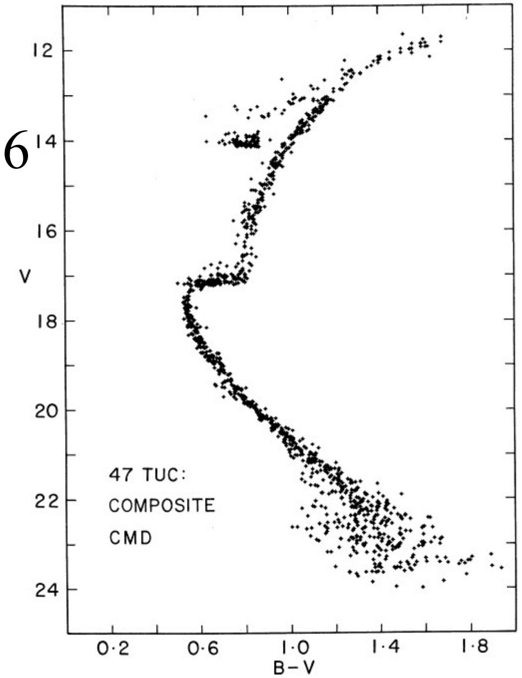

M15
[Fe/H]= -2.22

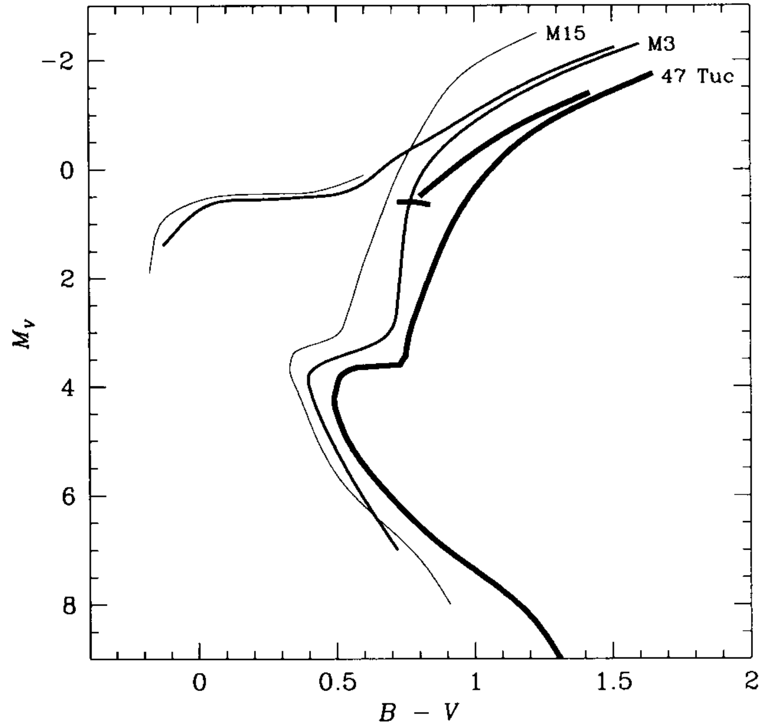

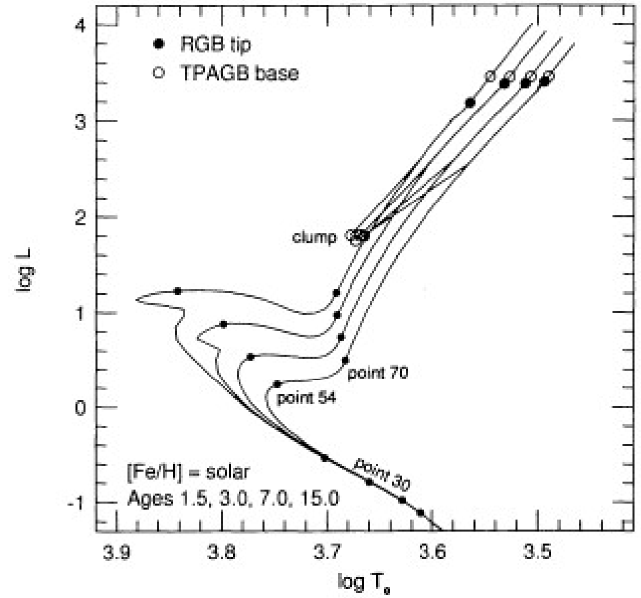

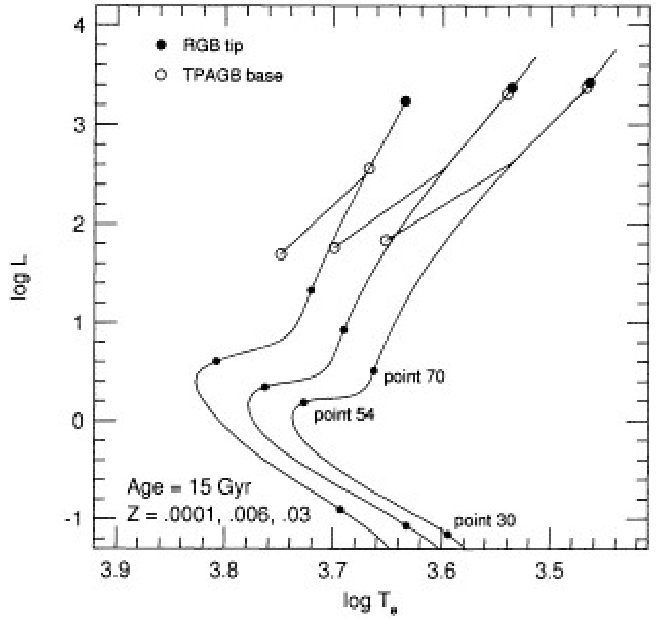

Worthey 1994, ApJS, 95, 107

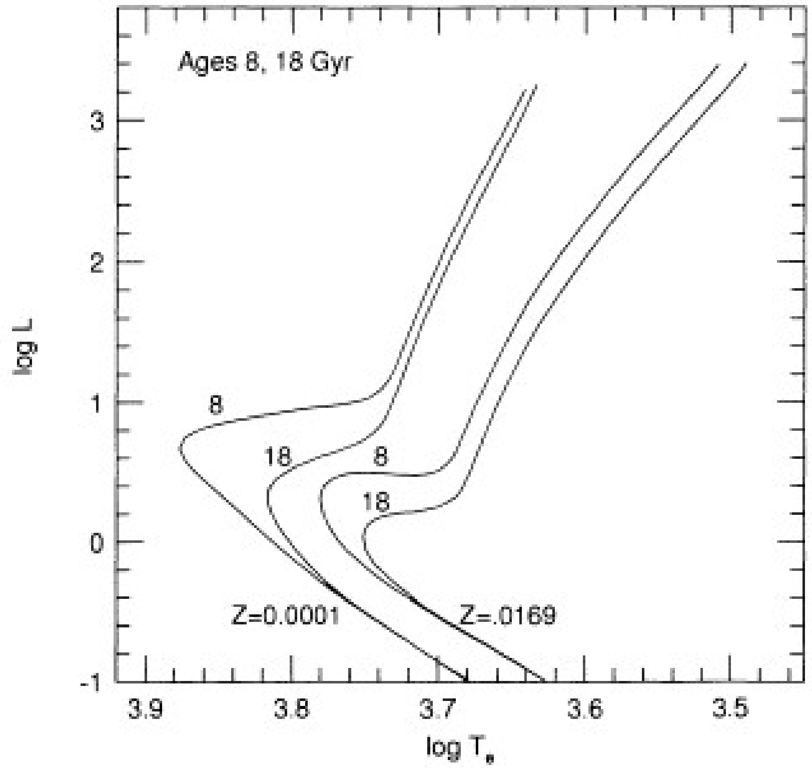

Age-metallicity degeneracy

Population synthesis of E galaxies

Worthey 1994, ApJS, 95, 107

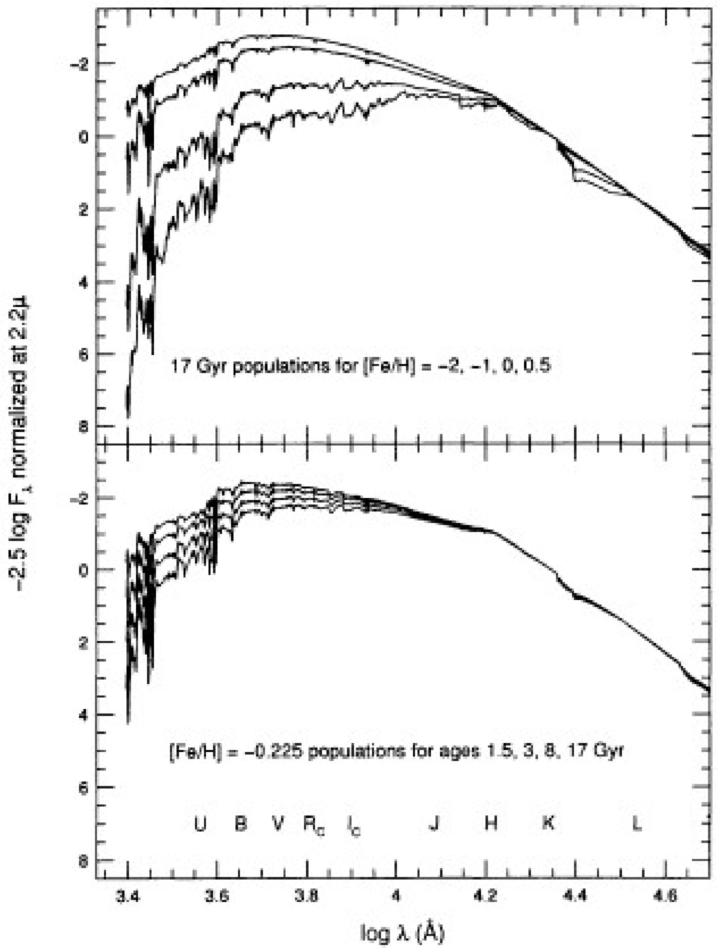

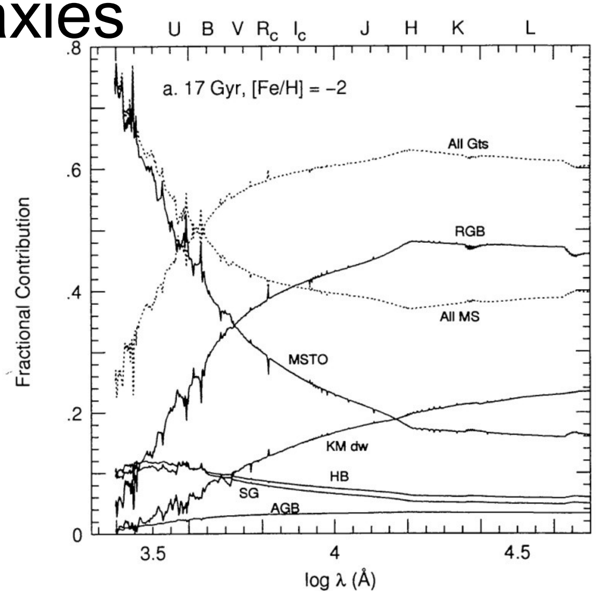

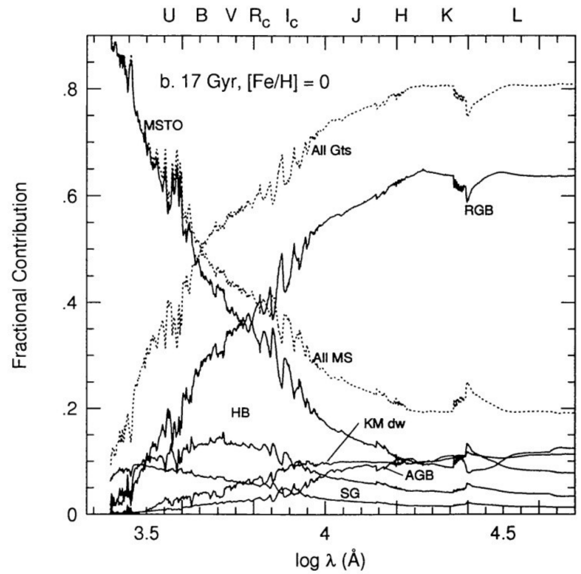

<u>Age-metallicity degeneracy</u>

Horizontal Branch (HB) morphology

M_{max} before He flash ~ 0.8 Msun
⇒ ~ 0.2 Msun must be lost until reaching HB

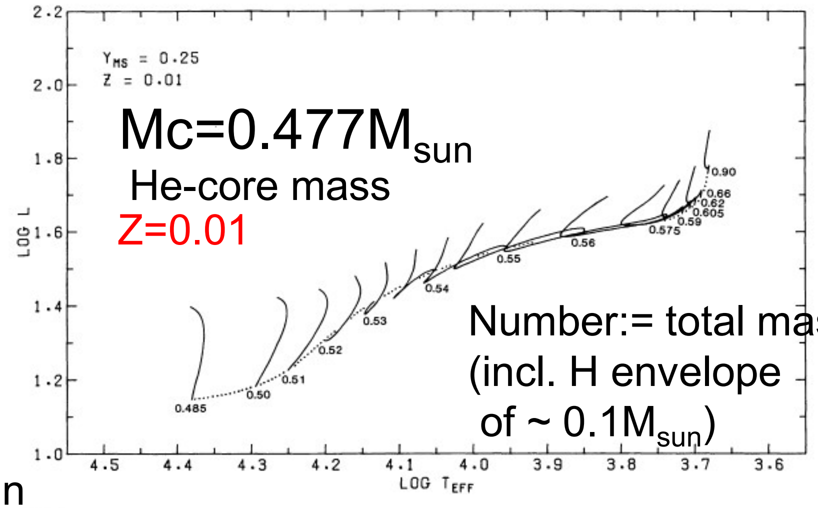

$Mc=0.477M_{sun}$
He-core mass
Z=0.01

Number:= total mass (incl. H envelope of ~ $0.1M_{sun}$)

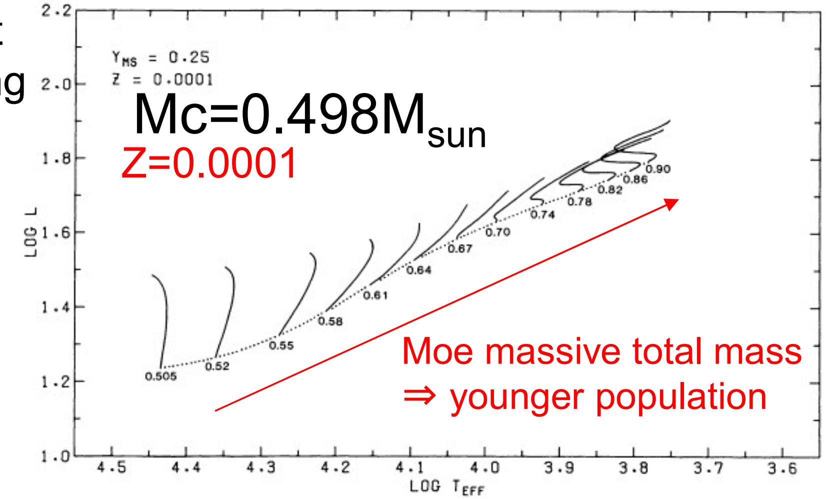

$Mc=0.498M_{sun}$
Z=0.0001

Moe massive total mass
⇒ younger population

Sweigart 1987, ApJS, 65, 95

Redder for more metal-rich stars

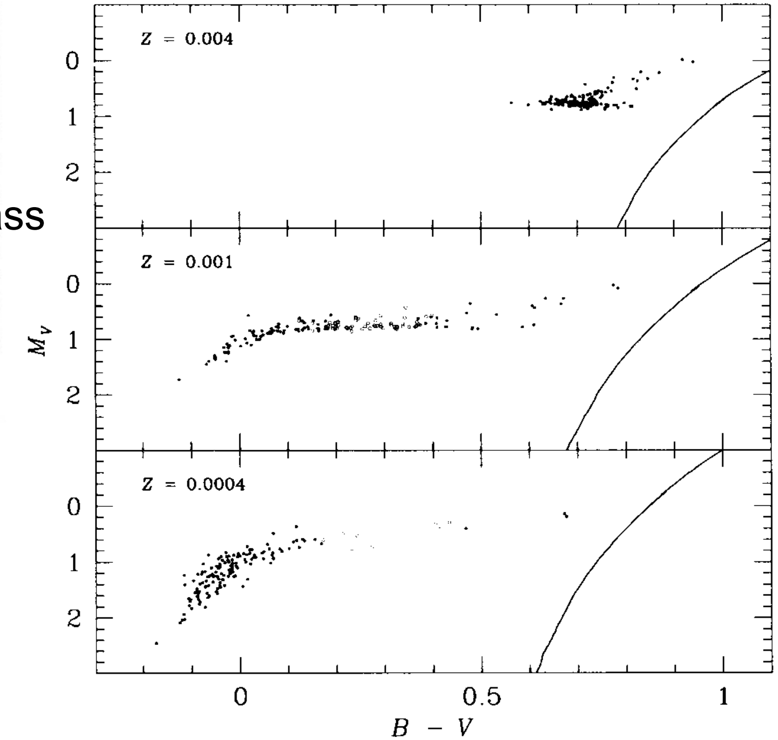

Lee et al. 1990, ApJ, 350, 155

t_{HB} ~ 0.1 Gyr

HB type (color) vs. metallicity in Galactic globular clusters

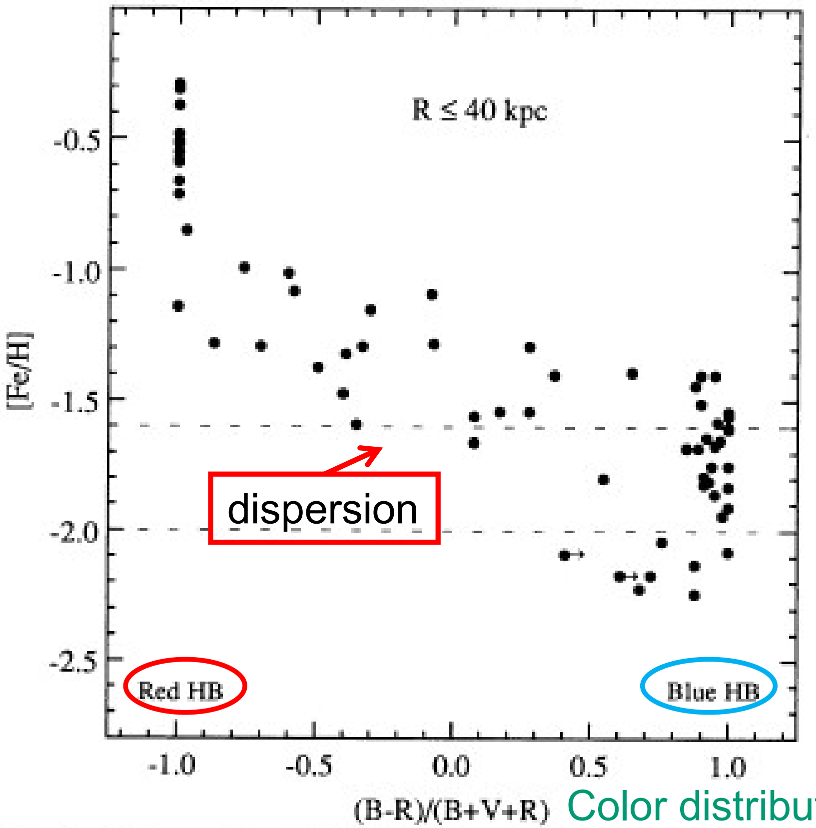

FIG. 2.—HB type, $(B-R)/(B+V+R)$, is plotted against [Fe/H] for all globular clusters with reasonably well-studied CM diagrams ($R \leq 40$ kpc). Note that the majority of clusters (e.g., M2, M13, M22) in the metallicity range $-2.0 \leq$ [Fe/H] ≤ -1.6 have very blue HBs [$(B-R)/(B+V+R) > +0.85$].

More red HBs
for higher [Fe/H]

B: # of blue HBs
R: # of red HBs
V: # of RR Lyrae

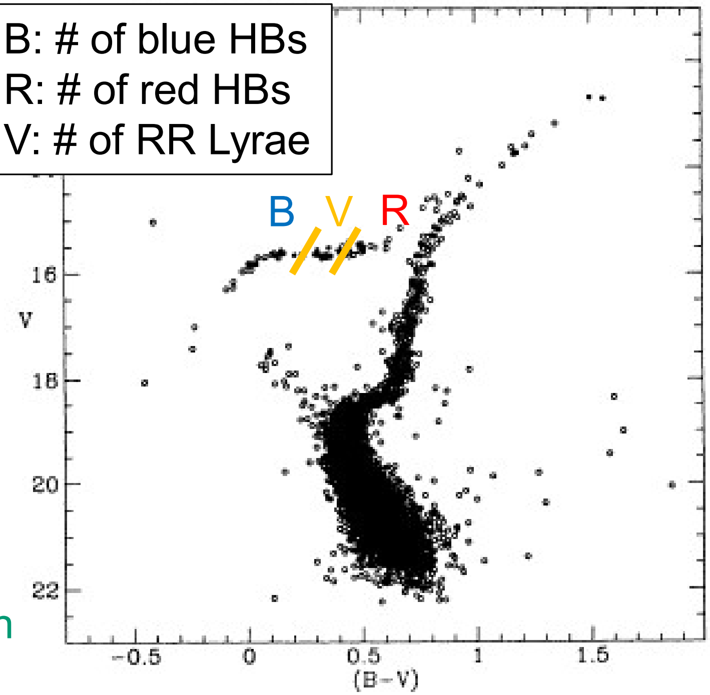

3. Origin of elements and yields

Type II SNe
M > 8 M_{sun}

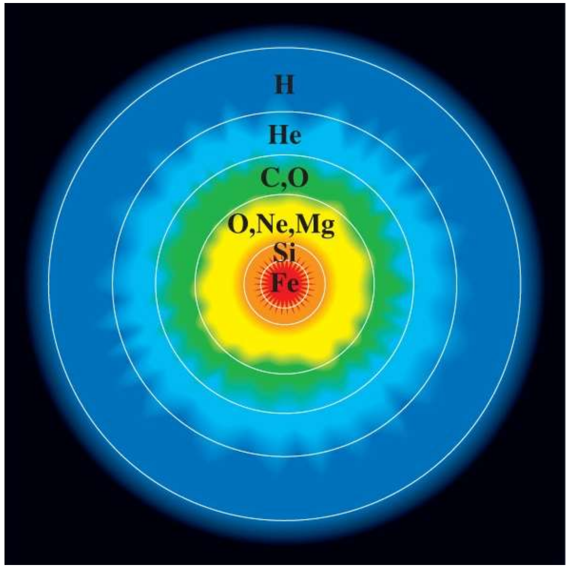

α-elements (O, Mg, Si)

Type Ia SNe
(white dwarf + companion)
M < 8 M_{sun}

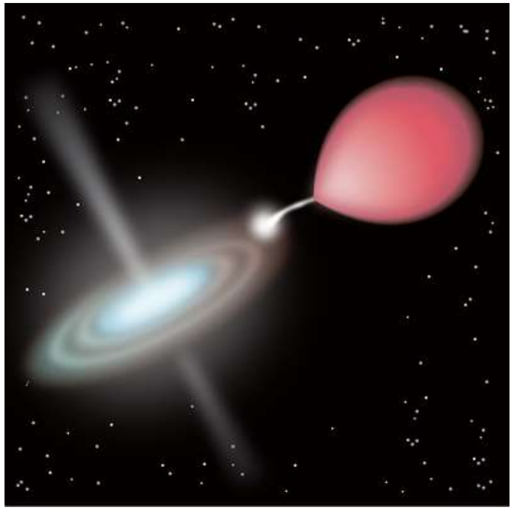

iron-peak elements

Origin of elements and yields

- $M<8M_{sun}$ (Type Ia SNe) white dwarf, mass accretion from a companion
  - Iron peak elements (Cr, Mn, Fe, Co, Ni)
- $M>8M_{sun}$ (Type II SNe) Core-collapse supernovae
  - α-elements (^{16}O, ^{20}Ne, ^{24}Mg, ^{28}Si, ^{32}S, ^{36}Ar, ^{40}Ca, ^{44}Ti)
  - $8<M<10M_{sun}$
    - C-burning、O+Ne+Mg-core、AGB star
    - O+Ne+Mg WD after losing H-He envelope or collapse due to e^- capture
  - $10<M<140M_{sun}$
    - Fe-core、gravitational collapse、neutron star or black hole
  - $140<M<300M_{sun}$ Pair-Instability SNe
    - Electron-positron pair creation & core collapse、high T_c & explosive O burning、disrupt out completely due to explosion, release a lot of Fe & Ca
  - $M > 300M_{sun}$
    - Photo-disintegration、core collapse, BH formation
- Hypernovae ($M>20M_{sun}$, $E>10^{52}$erg) gamma-ray burst
  - Large [Zn/Fe] & [Co/Fe] ratios

hydrostatic burning

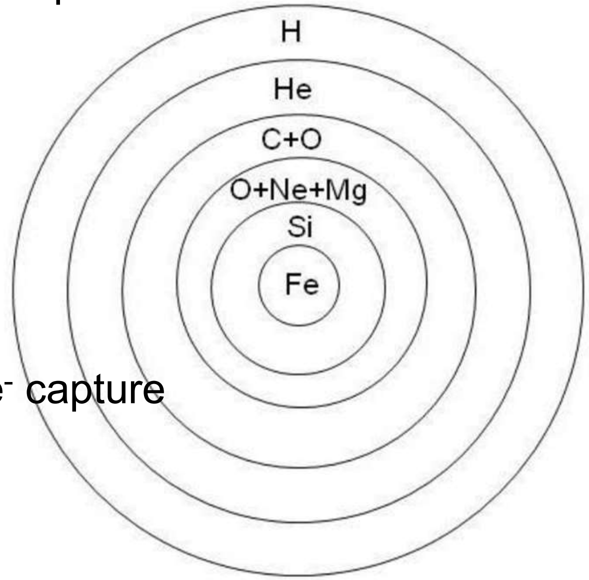

Supernova and Hypernova Yields

(Nomoto et al. 2009)

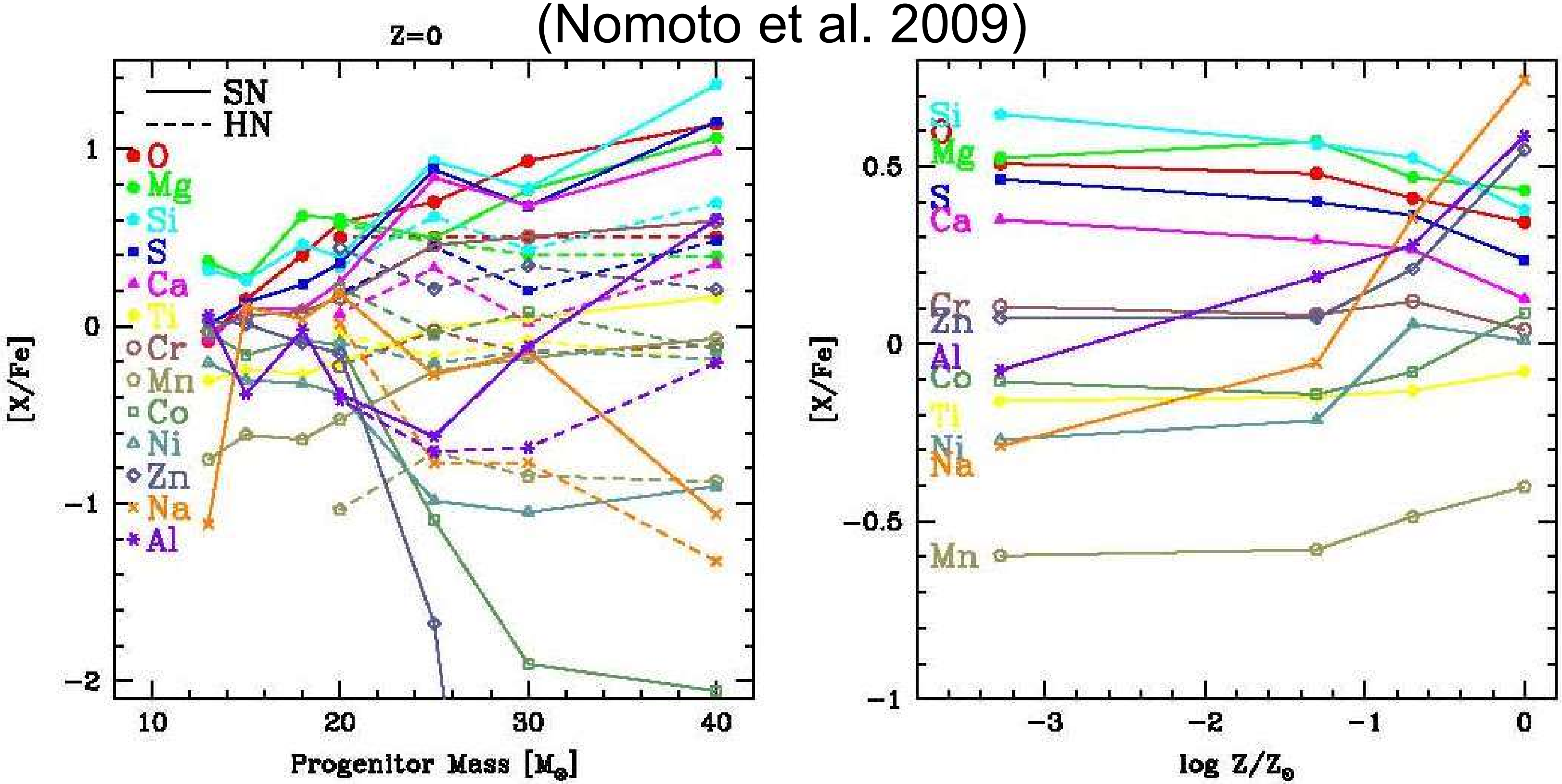

Figure 4. (*Left*:) Relative abundance ratios as a function of progenitor mass with $Z = 0$. The solid and dashed lines show normal SNe II with $E_{51} = 1$ and HNe. (*Right*:) The IMF weighted abundance ratios as a function of metallicity of progenitors, where the HN fraction $\epsilon_{\rm HN} = 0.5$ is adopted. Results for $Z = 0$ are plotted at $\log Z/Z_{\odot} = -4$ (Nomoto *et al.* 2006; Kobayashi *et al.* 2006).

Elements from Type II SN

α elements: ^{16}O, ^{20}Ne, ^{24}Mg, ^{28}Si, ^{32}S, ^{36}Ar, ^{40}Ca

Created at C- & O-burning phase

$^{12}C + ^{12}C \rightarrow ^{20}Ne + ^{4}He$, …

$^{20}Ne + ^{4}He \rightarrow ^{24}Mg + \gamma$, …

$^{16}O + ^{16}O \rightarrow ^{28}Si + ^{4}He$, …

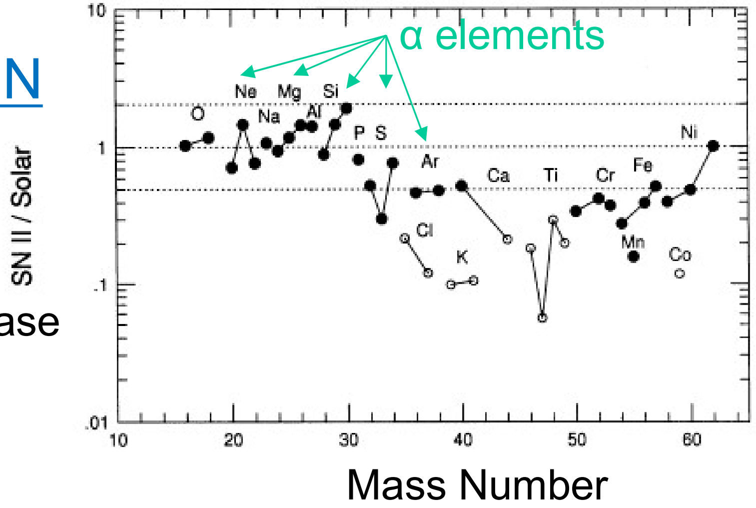

Figure 1. Abundance pattern from Type II supernova explosions. Relative abundances of synthesized heavy elements and their isotopes, normalized to the corresponding solar abundances, $x_i/x_i(\odot)$, are shown by circles. The species indicated by open circles are not used in minimizing $g(r)$ in equation (3), because of uncertainties involved in their abundances in Type II supernovae (see Section 2).

Tsujimoto et al. 1995, MN, 277, 945

Elements from Type Ia SN

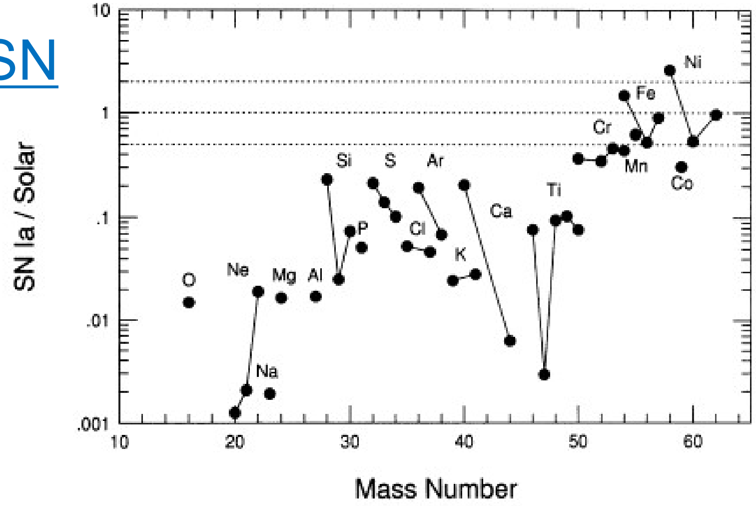

Figure 2. Abundance pattern from Type Ia supernova explosions. The relative abundances of synthesized heavy elements and their isotopes, normalized to the corresponding solar abundances, $x_i/x_i(\odot)$, are shown by circles.

Iron peak nuclides Cr, Mn, Fe, Co, Ni

Solar System Abundances

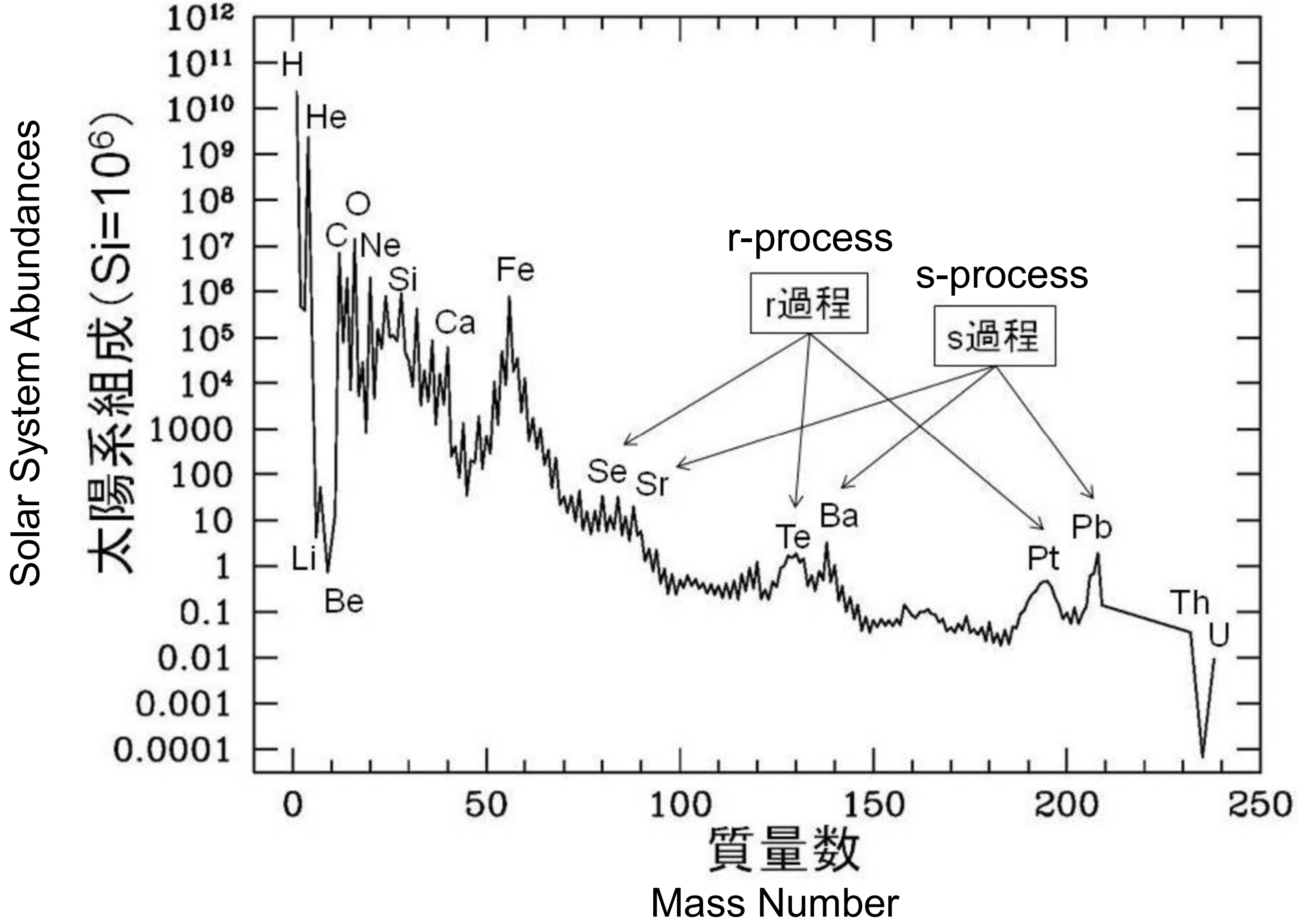

Big Bang Nucleosynthesis

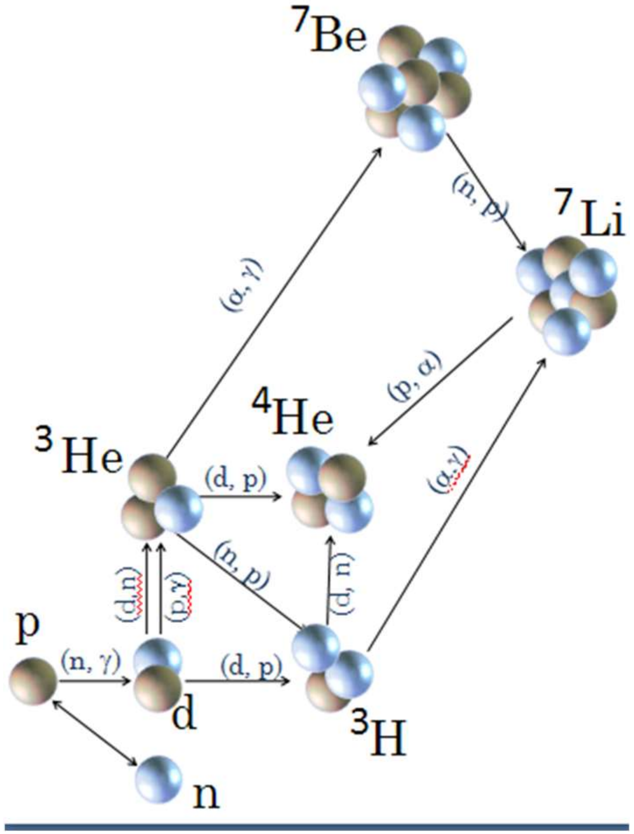

- p & n creation
- n + p → D + γ
  (D creation)
- D+D→^{3}H+p, ^{3}H+D→^{4}He+n
- After Big Bang
  H, D, ^{3}He, ^{4}He, ^{7}Li remained
  (^{7}Be, ^{3}H are unstable)

Big Bang Nucleosynthesis

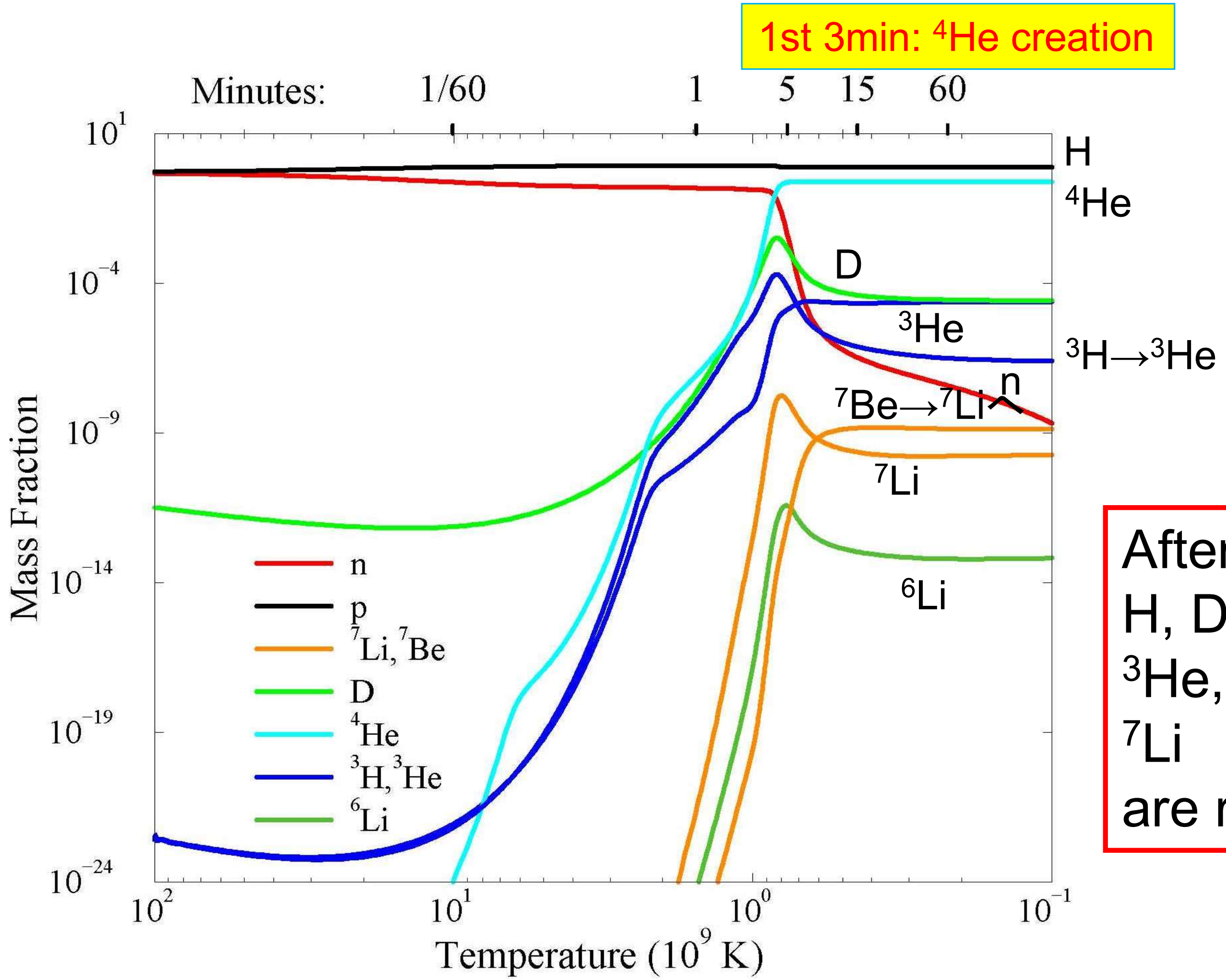

After big bang
H, D,
^{3}He, ^{4}He,
^{7}Li
are remained

Stellar evolution & nuclear reaction

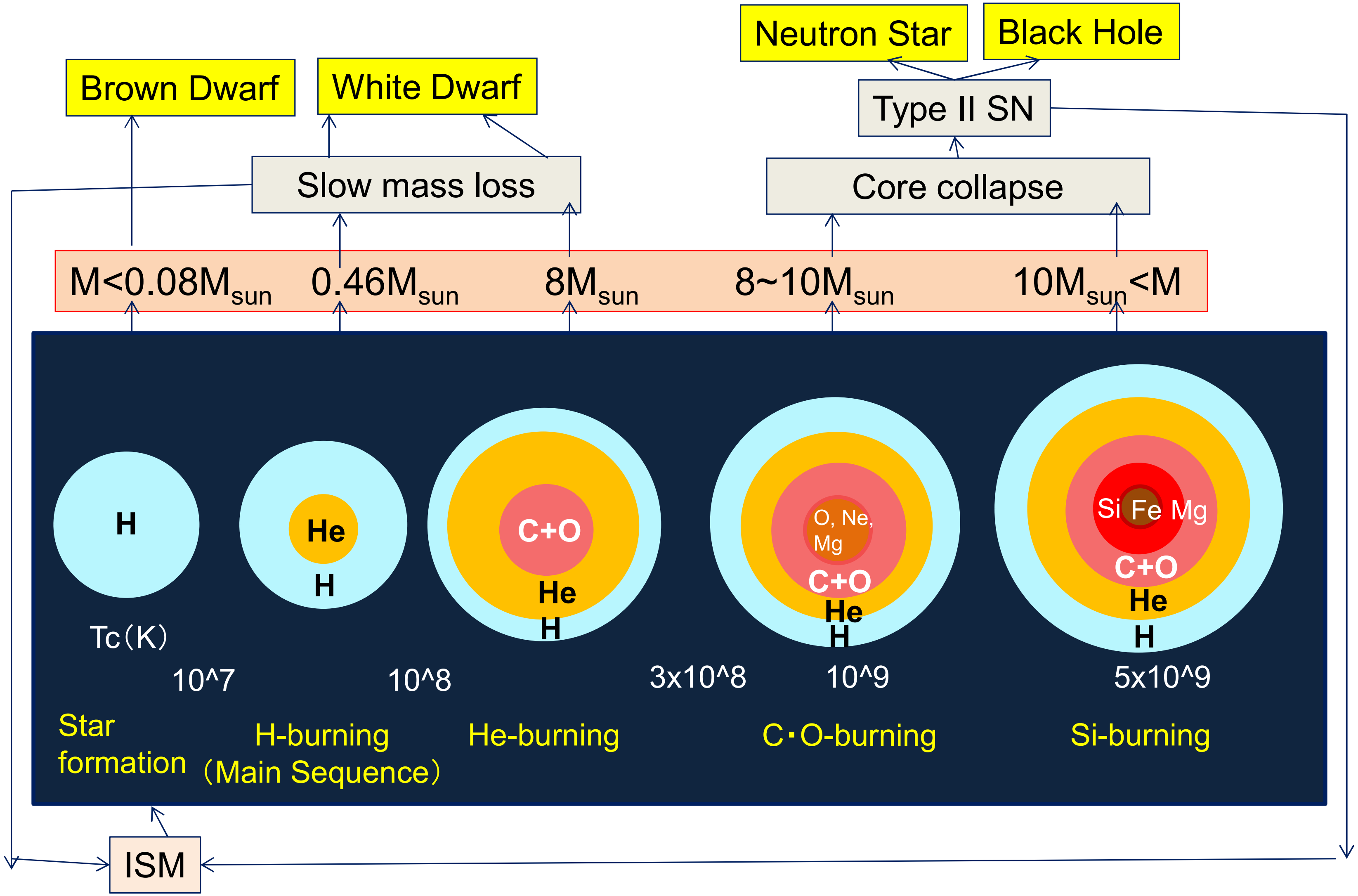

Origin of elements heavier than Fe
~ neutron capture process ~

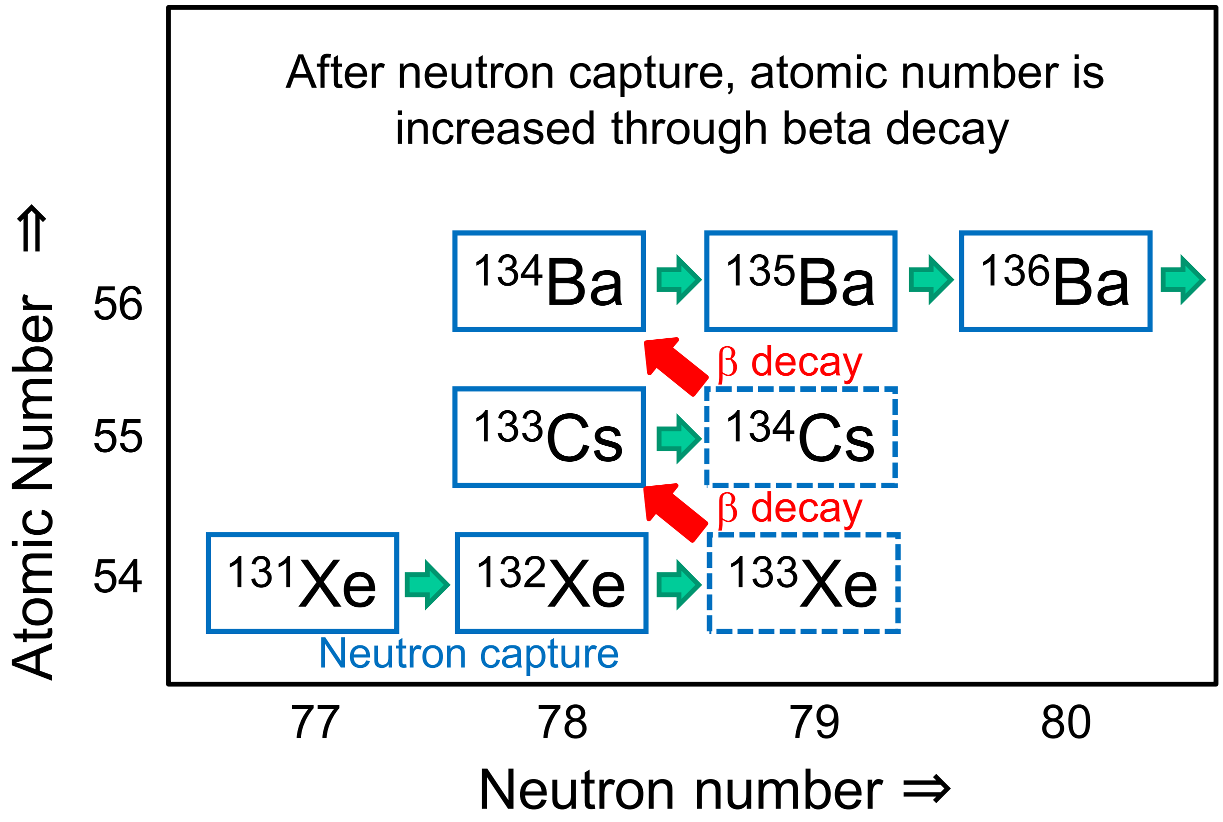

r-process

(τ < τ (β decay))

Eu, Pt, Au, Th, U

core-collapse SNe or merging of neutron stars

s-process

(τ > τ (β decay))

Sr, Ba, Pb

AGB stars

Neutron star mergers and r-process

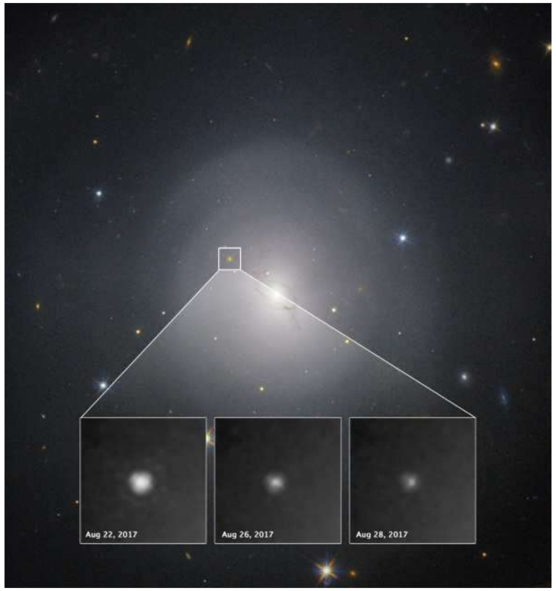

GW170817
Optically identified object

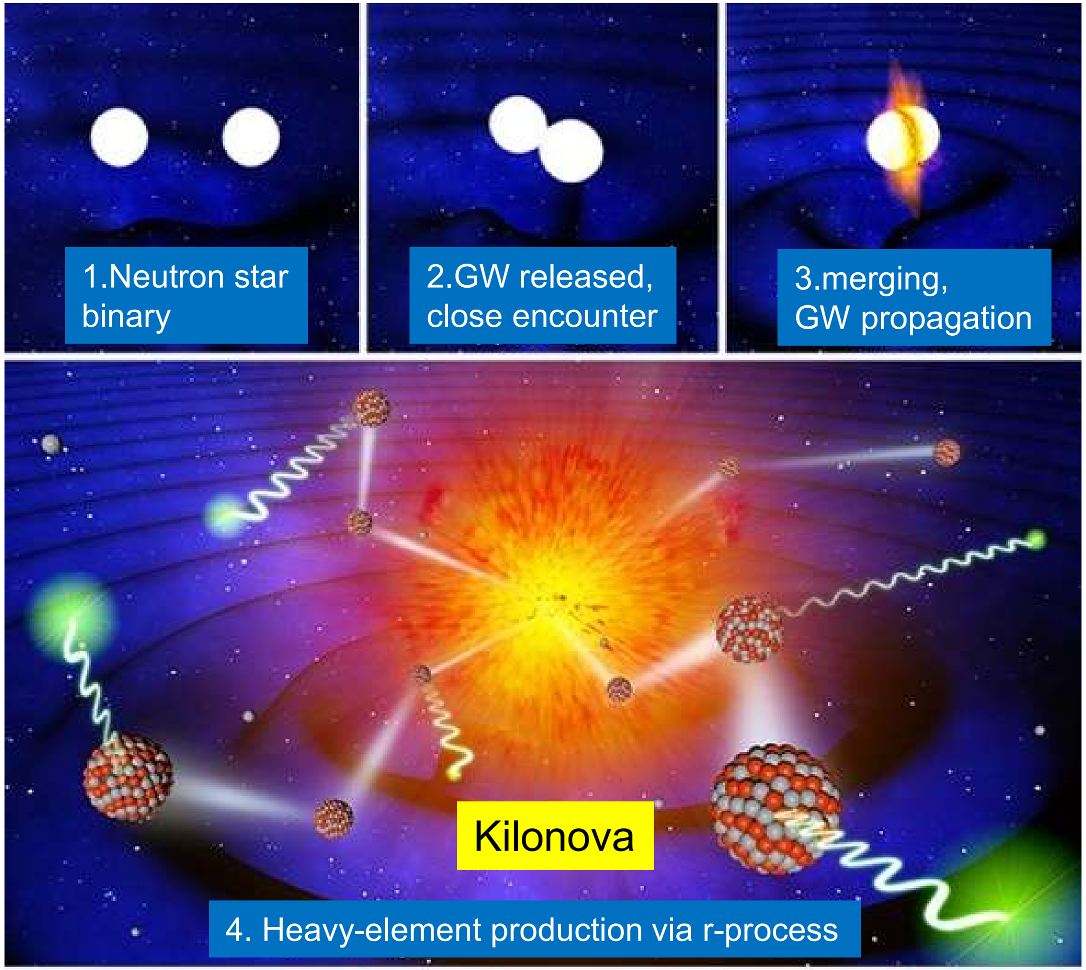

Solar System Abundances

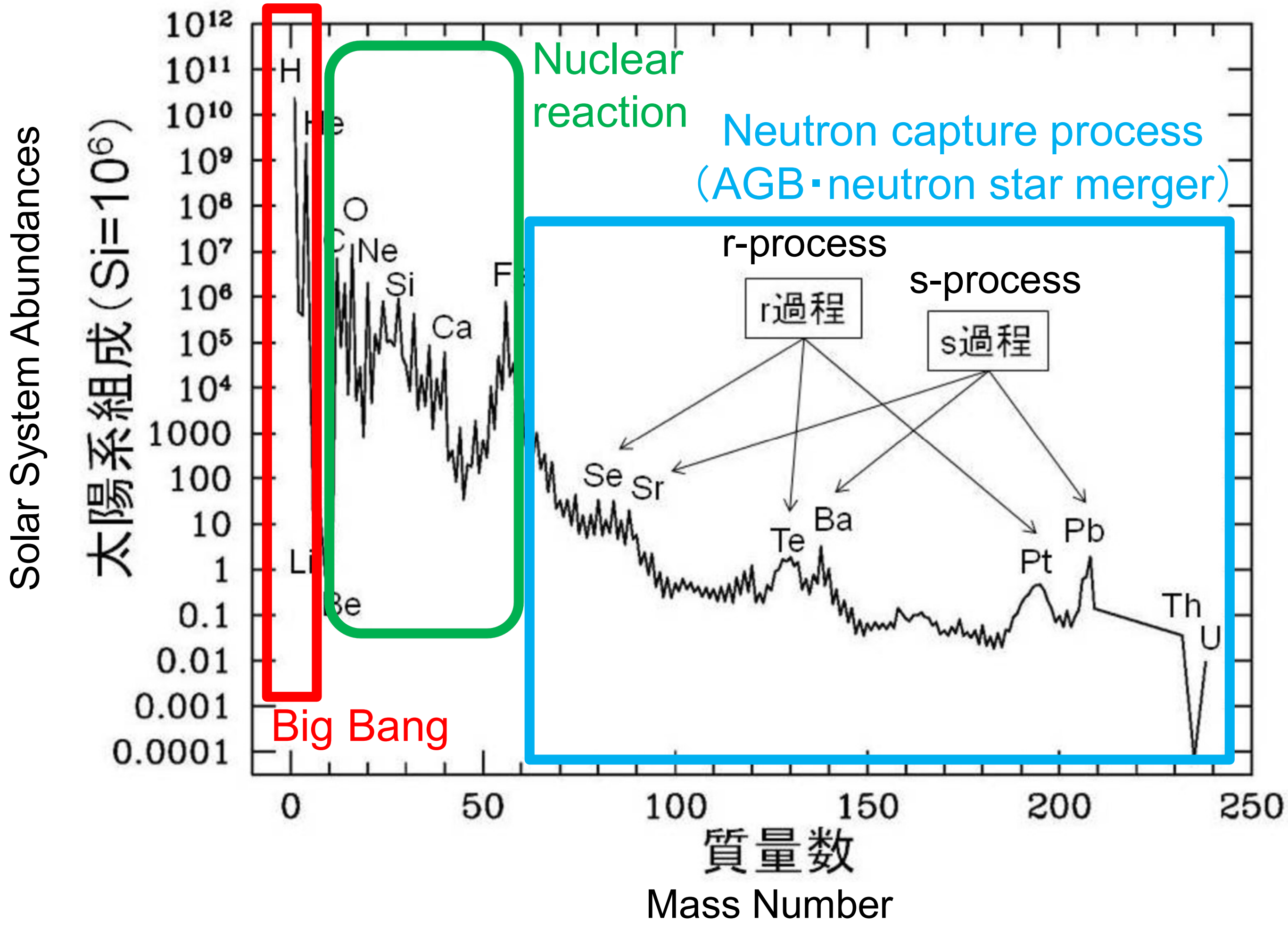

Where elements came from

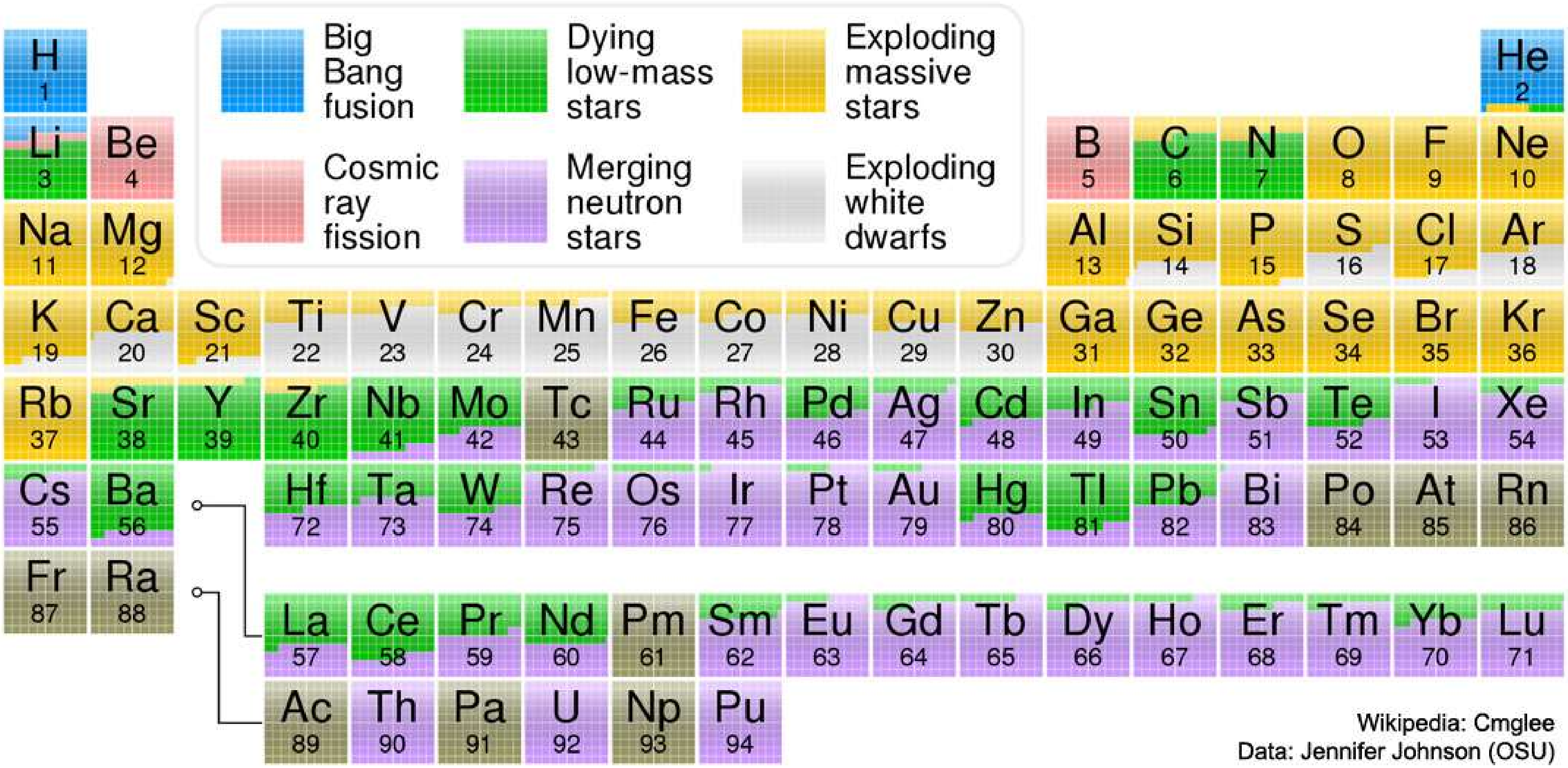

Wikipedia: Cmglee
Data: Jennifer Johnson (OSU)

Families of elements

1) Light odd-Z elements (Na and Al):
Mainly made in the hydrostatic burning shells of massive stars. Their yields are related to the mass of the shell, which is related to the initial mass of the star

2) Magnesium: Made in the hydrostatic burning shells of massive stars (specifically the C-burning shell), and the yield is related to the initial mass of the star.

3) The other alpha elements (O, Si, Ca, and Ti):
O is formed in a hydrostatic burning shell (the He-burning shell). The heavier alpha-elements Si, Ca and Ti are formed deep within massive stars during the explosive burning phase of a supernova (SN).

4) Fe-peak elements (Sc, V, Cr, Mn, Fe, Co, Ni, Cu and Zn):
With the exception of Cu and maybe Zn, these elements are made in both Type Ia and Type II SNe during the explosive phases. Co and possibly Zn are made almost exclusively in Type II SNe. Hypernovae is required for Zn.

5) Light s-process elements (Sr, Y, and Zr):
(Nearly all the elements heavier than Zn are made by neutron-capture processes.)
Made in metal-rich AGB stars. The peak of the s-process production moves to lighter elements as metallicity increases because there are more Fe-group "seed" nuclei at higher metallicity,

6) Heavy s-process elements (Ba and La):
Made in metal-poor AGB stars, although some of the inventory of both elements in the Sun came form the r-process.

7) r-process element (Eu):
By the explosive phase of Type II SNe or most probably merging of neutron stars.

List of elements and their production sites

- Lithium (Z=3): Produced in Big Bang nucleosynthesis and cosmic ray spallation.
- Carbon (Z=6): Results from the triple-alpha He-burning process. Isotope ratios between ^{12}C and ^{13}C are affected by hydrogen burning on the CNO cycle.
- Oxygen (Z=8): Results from hydrostatic He-burning burning in massive stars, yield related to the mass of the He-burning shell, which is a function of the star's initial mass.
- Sodium (Z=11): Results mostly from carbon-burning. Production depends on the n/p ratio, so there is a predicted metallicity dependence of the yield from SN II. Can also be affected by H-burning in intermediate-mass stars, as seen in the so-called "Na-O anti-correlation" often seen in globular cluster stars.
- Magnesium (Z=12): Results from carbon-burning. Effectively $^{12}C \rightarrow {}^{24}Mg$ via $^{20}Ne + {}^{4}He$. Released from SN II.
- Aluminum (Z=13): Carbon-burning; closely tied to the production of the minor Mg isotopes $^{25,26}Mg$. Production depends on the n/p ratio, so there is a predicted metallicity dependence of the yield from SN II. Can also be affected by H-burning in intermediate-mass stars, as seen in "Na-O anti-correlation" in globular cluster stars.

Correlated strongly to C+N initial abundance

- Silicon (Z=14): Explosive oxygen burning via 2O→Si + He, with Mg + He→Si. SN II+SN Ia.
- Calcium (Z=20): Oxygen and silicon burning, both hydrostatic and explosive. SN II.
- Scandium (Z=21): SN II from oxygen burning + the alpha-rich freezeout.
- Titanium (Z=22): Explosive Si burning, + alpha-rich freezeout, including white dwarfs (SN Ia). Appears to be mostly SN II.

- Vanadium (Z=23): Explosive oxygen burning + silicon burning. SN Ia probably dominate production. The [V/Fe] value is very sensitive to the value of Teff.
- Chromium (Z=24): Equilibrium process in explosive Si burning. SN II + SN Ia, but dominated by SN II.
- Manganese (Z=25): Explosive Si burning + alpha-rich freezeout. SN II. Metallicity dep.
- Iron (Z=26): Equilibrium process. SN II + SN Ia, with a large yield from SN Ia.
- Cobalt (Z=27): Explosive Si burning + alpha-rich freezeout (which produces a large Co/Fe yield). Possibly metallicity-dependent yields in Type II SN.
- Nickel (Z=28):. Explosive Si burning + alpha-rich freezeout. SN II + SN Ia
- Copper (Z=29): Possibly from SN II "only" with metallicity-dependent yields. Minor contributions from the s-process and SN Ia.
- Zinc (Z=30): Explosive Si burning + alpha-rich freezeout + s-process. Zn does not form on dust grains, so it is used in the study of damped Lyman-alpha systems as metallicity indicator.
- Strontium (Z=38), Yttrium (Z=39), Zirconium (Z=40), Molybdenum (Z=42), and Palladium (Z=46): Light s-process. AGB stars and maybe massive stars ("weak s-process").
- Barium (Z=56): Heavy s-process. AGB stars. [heavy s/light s]= f(Z).
- Lanthanum (Z=57): Heavy s-process. AGB stars. [heavy s/light s]= f(Z).
- Europium (Z=63): Bypassed by s-process (mostly), best r-process "only" element in the optical. The r-processes were believed to occur in a sub-class of SN II, the lower-mass SN II, but now the merging of neutron stars is thought to be most likely.

4. Extremely metal-poor stars

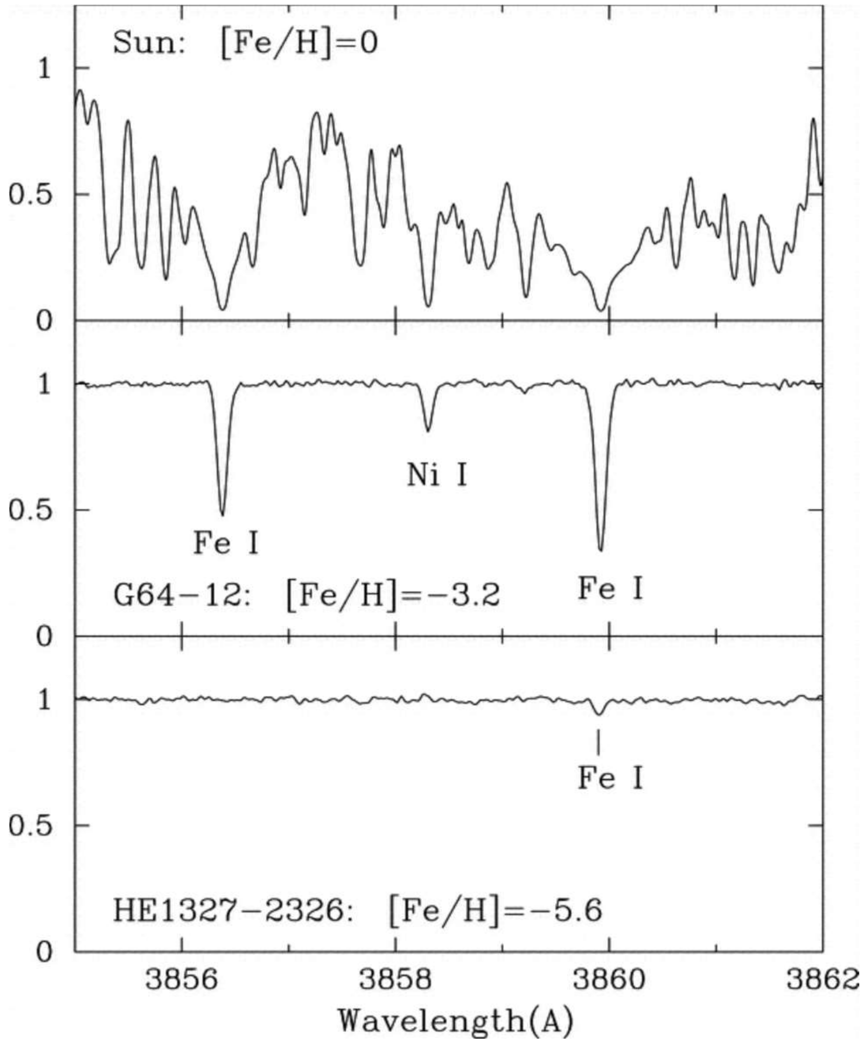

[Fe/H] ≤ -2.5

These stars were enriched by just one supernova.

↓

Their abundance patterns reflect the mass of a progenitor star (first star).

Abundance ratios

Dispersion due to difference in progenitor's mass
+ inhomogeneous
  chemical evolution

[Mg/Fe]

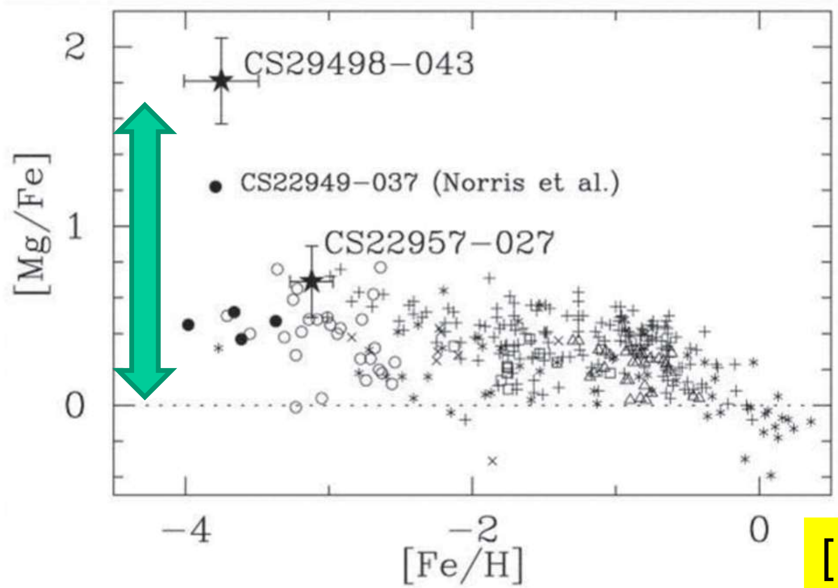

Aoki et al. (2002)

[Fe/H]

[Eu/Fe]

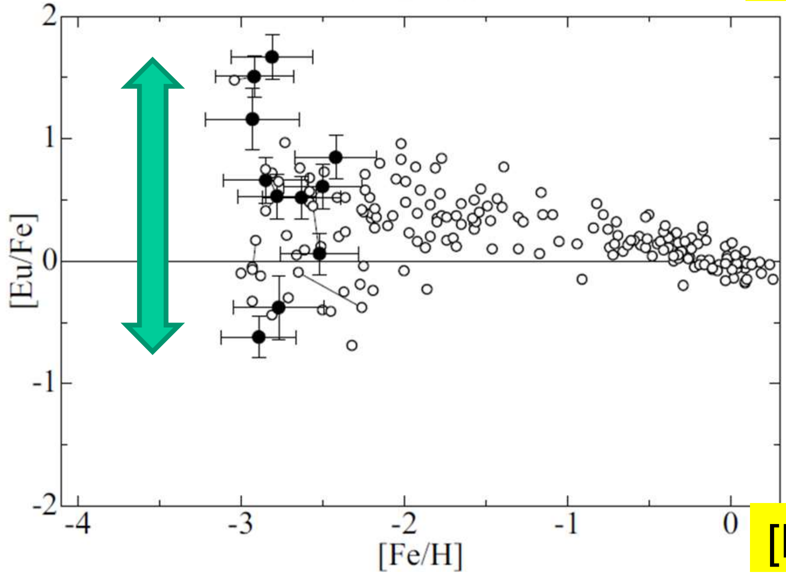

Honda et al. (2004)

[Fe/H]

r-process elements
for a star with [Fe/H]=-3.1

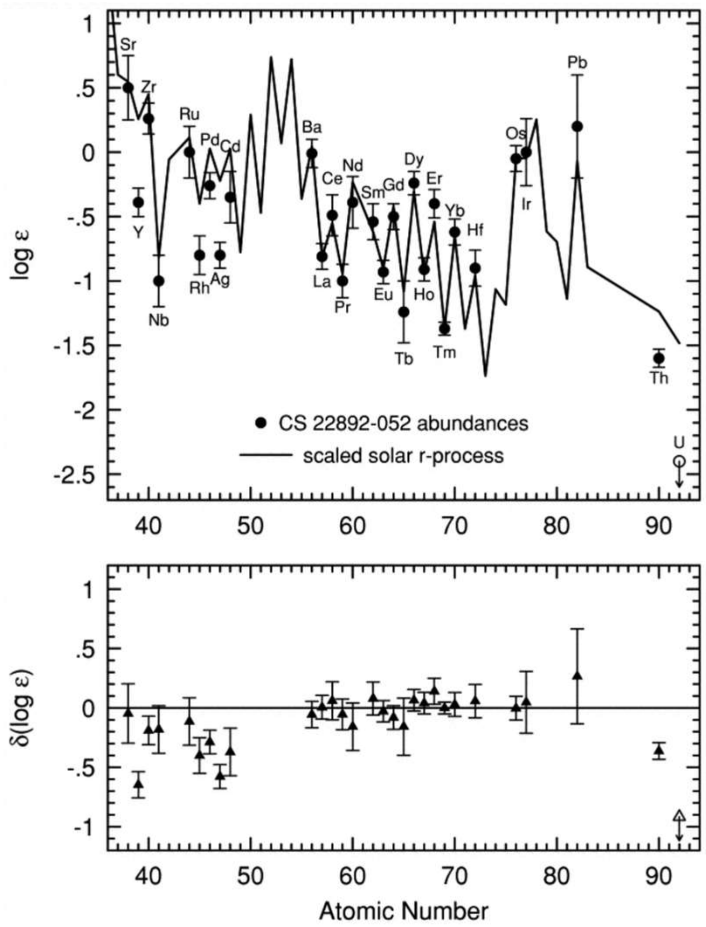

s-process elements
for a star with [Fe/H]=-2.7

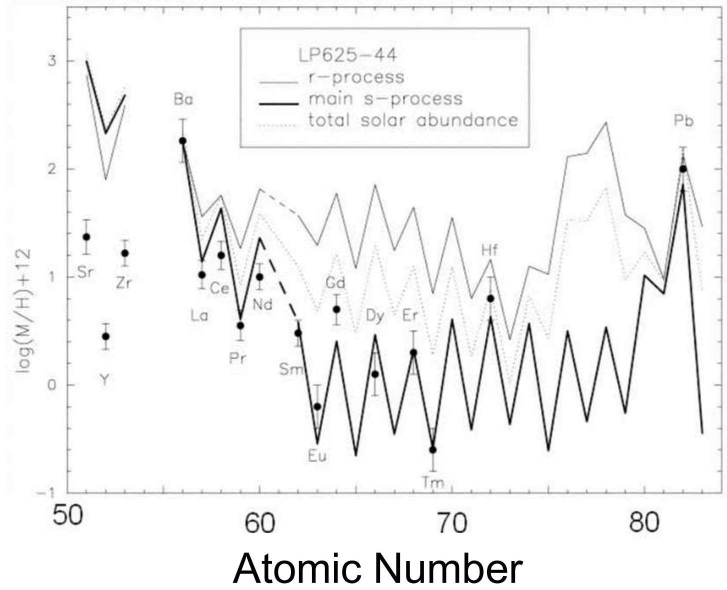

Carbon-enhanced extremely metal-poor star
(CEMP stars)

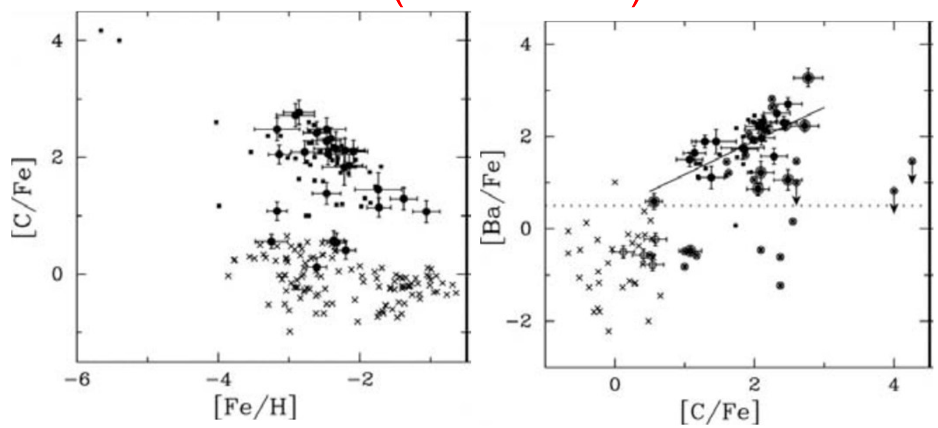

Universal mechanism (by SNe II
or merging of neutron stars)
is at work for r-process.

Nucleosynthesis from Hypernovae
(Tominaga et al. 2007)

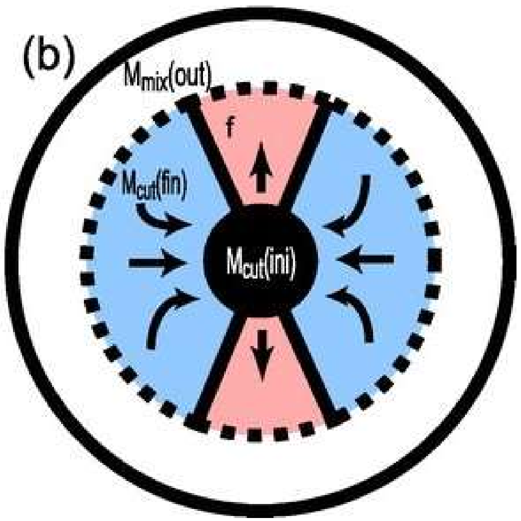

Mixing-fallback model

M=25M_{sun}, E=10^{52} erg

[X/Fe]

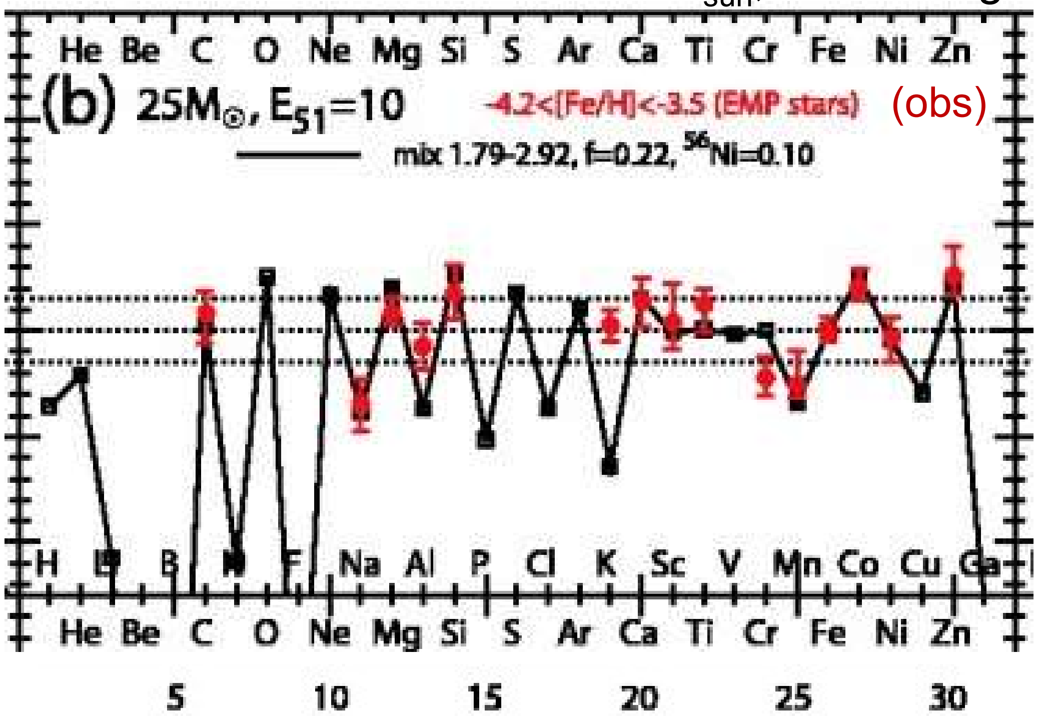

Z

Observed large [Zn/Fe] & [Co/Fe] ratios are reproduced.

5. Galactic chemical evolution

- Simple model
  - Key parameters: SFR: $\psi(t)$, IMF: $\phi(m)$

    $\phi(m) \propto m^{-\alpha}$ ($\int m\phi(m)dm = 1\ M_{sun}$)
  - star: M_s, gas: M_g, metal: M_z, metallicity: $Z=M_z/M_g$
  - closed box: $M_{tot} = M_s+M_g$ = const.
  - instantaneous recycling: Massive stars die immediately and leave enriched gas (age: $\tau \ll 1$).

    The rate of gas ejection is:

$$\int_{m_1}^{\infty}(m-w_m)\,\varphi(m)\psi(t-\tau(m))dm \rightarrow \int_{m_1}^{\infty}(m-w_m)\varphi(m)\psi(t)dm \equiv R\psi(t)$$

    w_m: remnant mass, R: return fraction
  - y: yield

    metallicity when a unit gas mass is locked into stars

$$\begin{cases} \dfrac{dM_g}{dt} = -\dfrac{dM_s}{dt} = -\psi + R\psi = -(1-R)\psi \\ \dfrac{d(ZM_g)}{dt} = -Z(1-R)\psi + y(1-R)\psi \end{cases}$$

$$\Rightarrow Z = y \ln \frac{M_{tot}}{M_g} = y \ln f_g^{-1}$$

f_g: gas fraction <1
→ Z increases with decreasing f_g

$$S(Z) = \frac{M_s}{M_{s,current}} = \frac{1-f_g}{1-f_{g,current}} = \frac{1-f_{g,current}^{Z/Z_0}}{1-f_{g,current}}$$

S(Z): cumulative metallicity distribution of stars

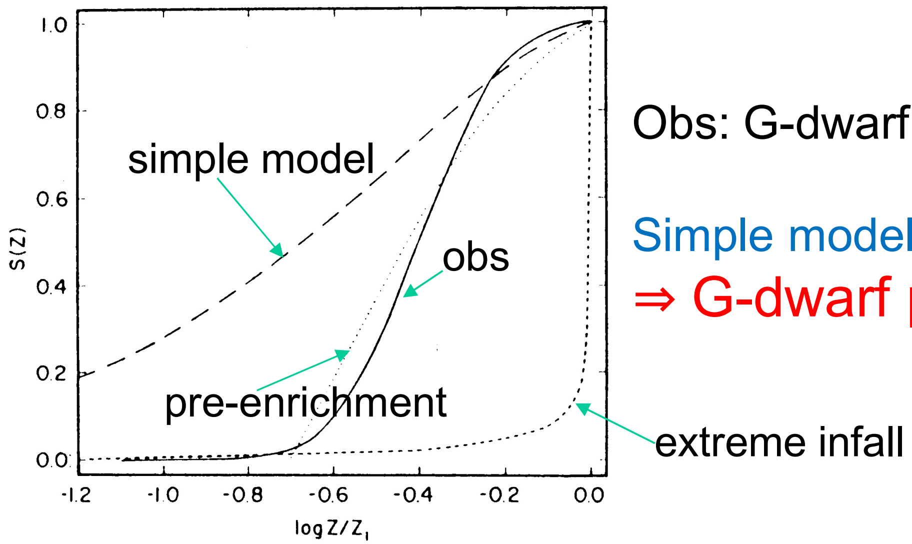

Obs: G-dwarf stars near the Sun

Simple model: too many metal-poor stars
⇒ G-dwarf problem

Tinsley 1980, FCPs, 5, 287

Gaseous Oxygen abundance in M81
Garnett & Shields 1987, ApJ, 317, 82

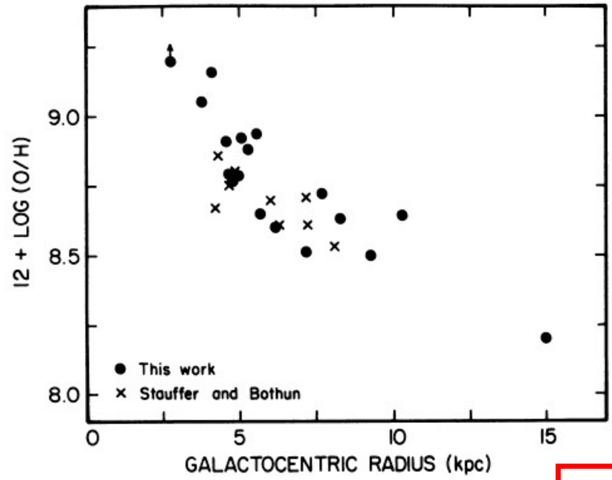

Gaseous Oxygen in various galaxies

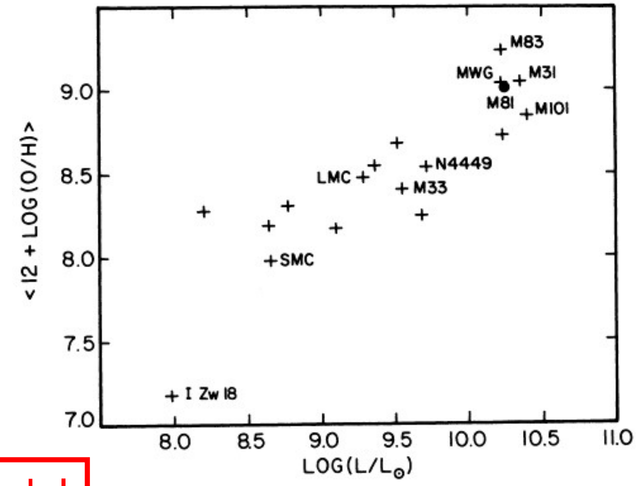

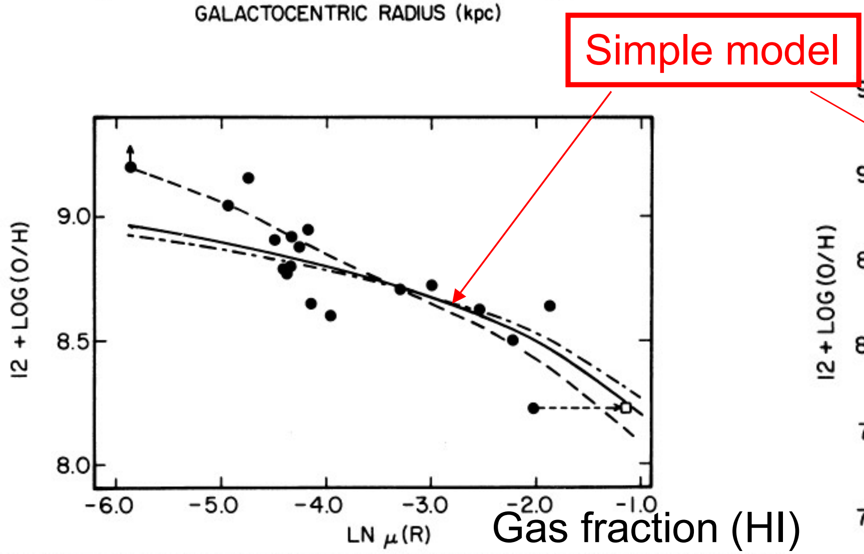

FIG. 9.—O/H vs. the log of the H I gas fraction for H II regions in M81. The solid line represents the results from the "simple" chemical evolution model with yield $y = 0.004$; the dot-dash line gives $Z^*(\mu)$ from Clayton (1986) with $y = 0.0055$, while the dashed line shows the predictions from the variable-yield model of Edmunds and Pagel (1984). The square marks the position of Münch 1 if the surface density is computed from an extrapolation of the exponential disk.

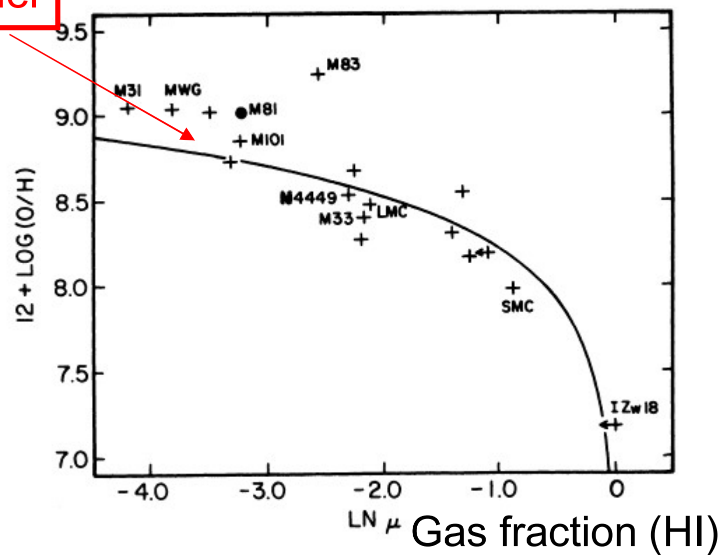

SFR law for 61 disk galaxies and 36 starburst galaxies

Kennicutt 1998, ApJ, 498, 541

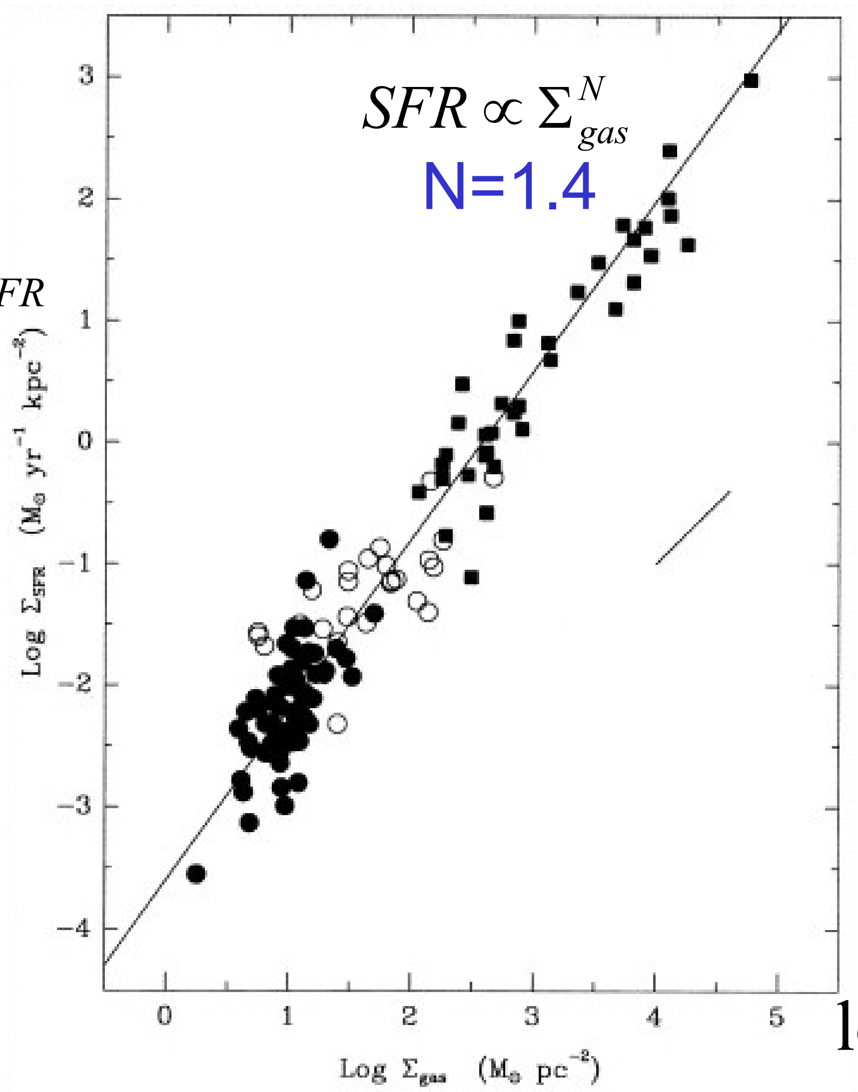

Initial Mass Function

$\phi(m) \propto m^{-\alpha}$ ($\int m\,\phi(m)dm = 1M_{sun}$)

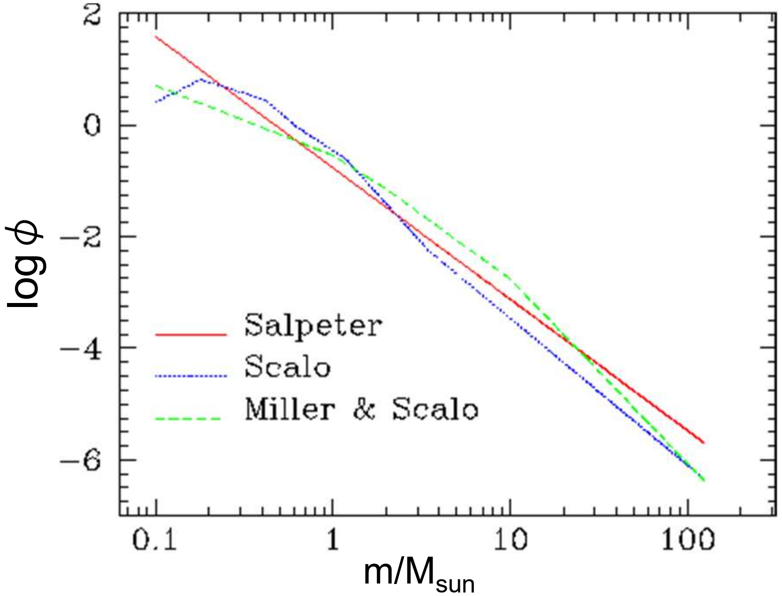

Kroupa (2002)

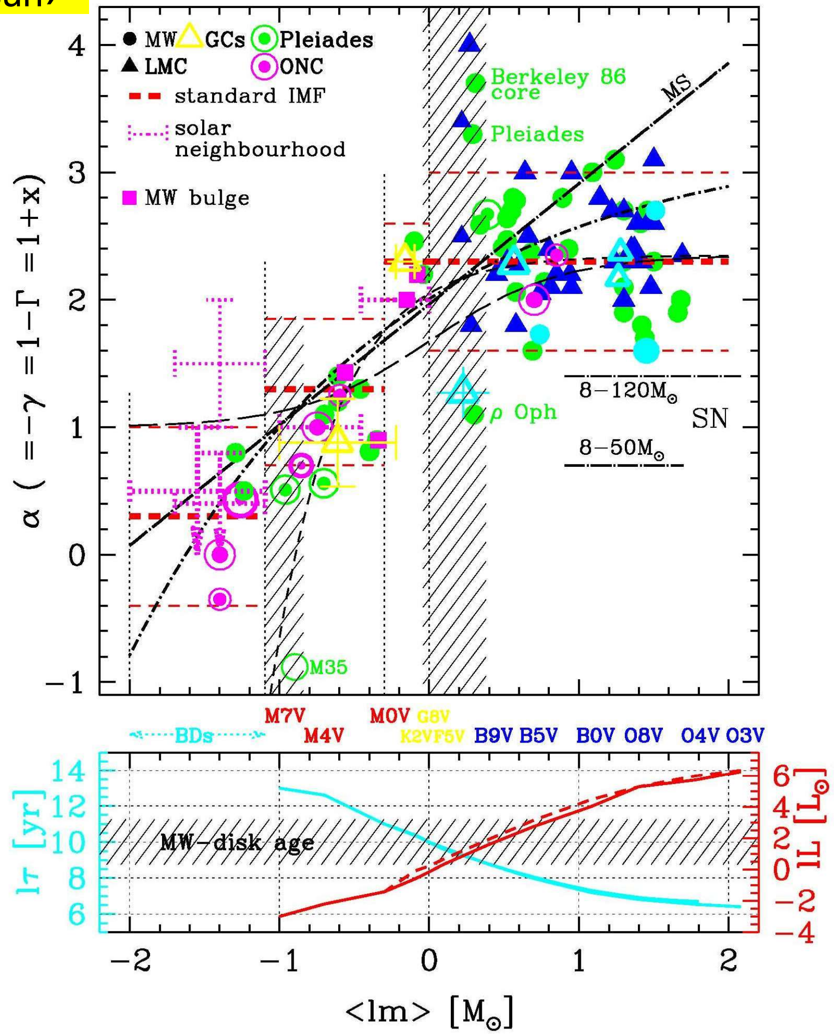

- Salpeter (1955)
  α = 2.35 for $1M_{sun} < m$
- Miller and Scalo (1979), Scalo (1986)
  $\alpha \to 0$ for $m < 1M_{sun}$
- Kroupa (2002)
  α = 0.3 for $m < 0.08M_{sun}$
  1.3 for $0.08 < m < 0.5M_{sun}$
  2.3 for $0.5M_{sun} < m$

MDF of G-dwarfs in the solar neighborhood

(model: Sommer-Larsen & Yoshii 1990, MN, 243, 468)

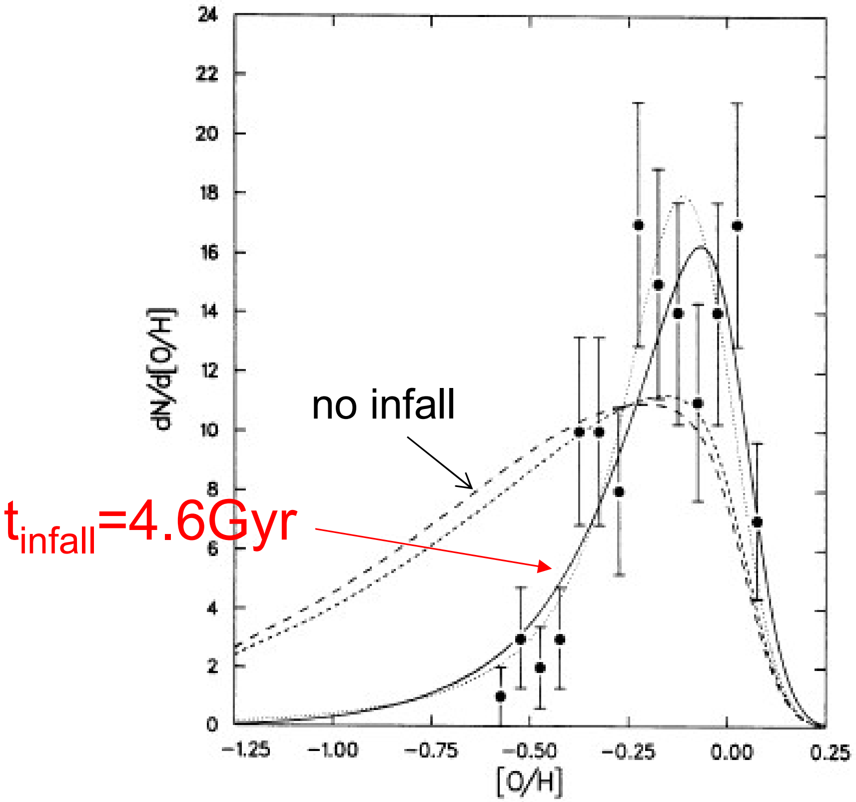

$d\Sigma_{gas}/dt \propto \exp(-t\ /\ t_{infall})$

t_{infall}~4-5 Gyr is required

The Galactic (thin) disk formed slowly over 4-5 Gyr.

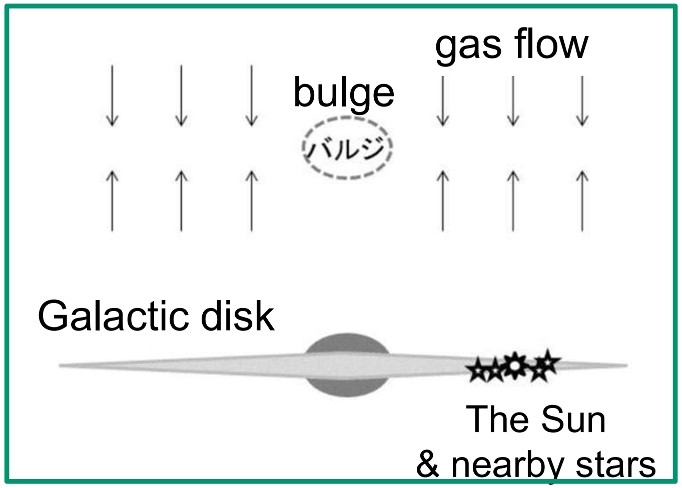

Chemical clock

[α element/Fe]

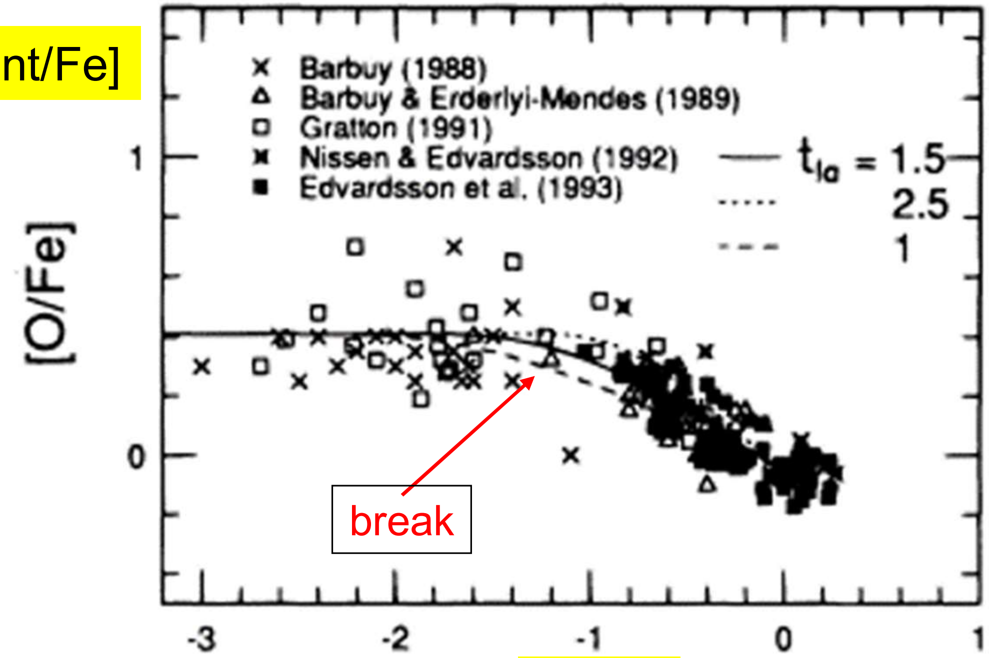

[Fe/H]

Pace of chemical enrichment (or SFR)

Yoshii et al. 1996, ApJ, 426, 266

Time scale for
Type Ia SN :
~ 1 Gyr
(at [Fe/H] ~ -1
near the Sun)

Comparison with metallicity distribution (MD) of young stars (B-type stars)

Feltzing & Chiba (2013)
using Nieva and Przybilla (2012) data

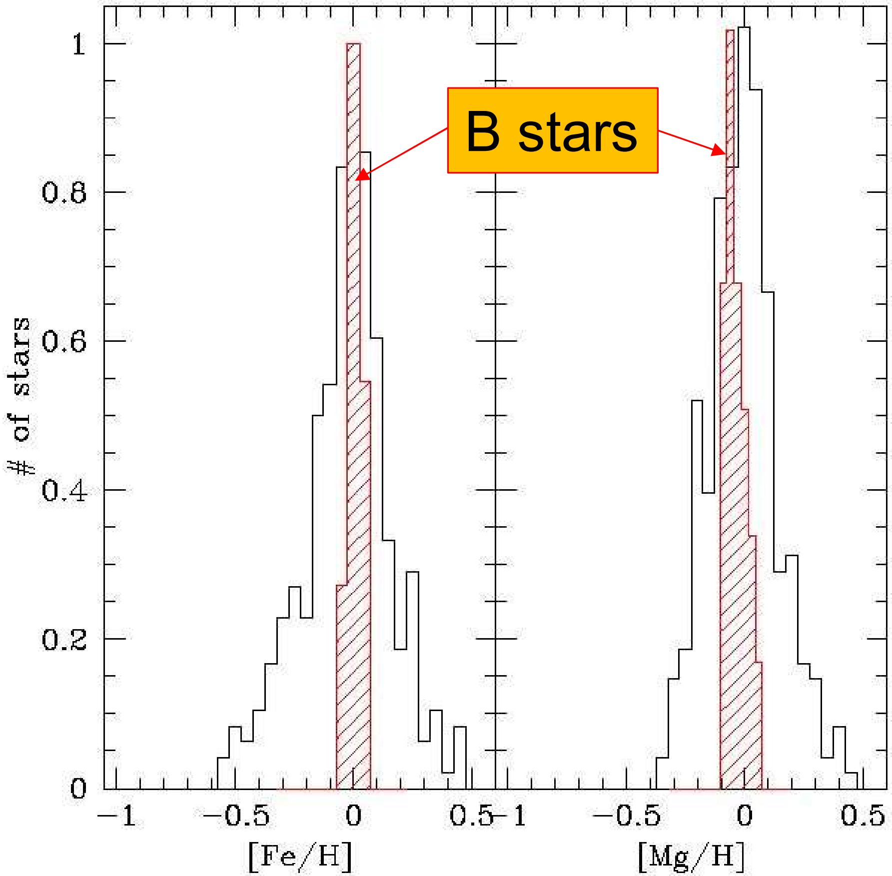

MD of B-type stars reflects that of ISM near the Sun

Very meal-rich stars with [Fe/H] > + 0.2 cannot be formed near the Sun

These very metal-rich stars (possibly having exo-planets) are migrated from inner radii

Radial migration of stars

Sellwood & Binney 2002, Schoenrich & Binney 2009

- Epicycle motion
- Angular-momentum transfer by transient spiral arms

Radial migration of stars

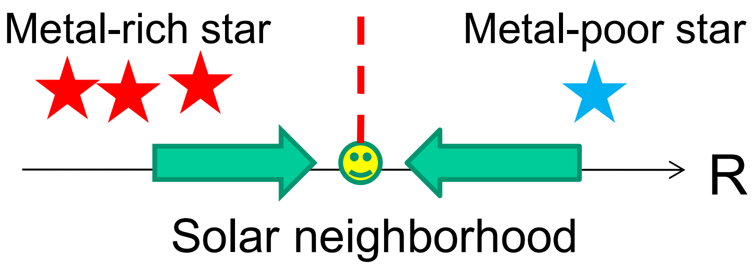

$Lz = V_{\varphi} R \sim const.$
Star moving from inner R： V_{φ} is slower
Star moving from outer R： V_{φ} is faster

[α/Fe] ratios in several MW dSphs

(Tolstoy+ 2009)